

**UNIVERSITY OF GAZIANTEP
GRADUATE SCHOOL OF
NATURAL AND APPLIED SCIENCE**

**STABILITY ASSESSMENT OF SEYRANTEPE CAVES IN
GAZIANTEP**

**M. Sc. THESIS
IN
CIVIL ENGINEERING**

**BY
SERDAR ALLI
JUNE 2014**

Stability Assessment of Seyrantepe Caves in Gaziantep

**M. Sc. Thesis
in
Civil Engineering
University of Gaziantep**

**Supervisor
Assoc. Prof. Dr. Hanifi ÇANAKÇI**

**By
Serdar ALLI
June 2014**

©2014 [Serdar ALLI].

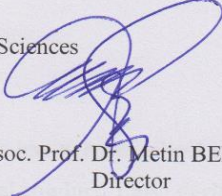
T.C.
UNIVERSITY OF GAZİANTEP
GRADUATE SCHOOL OF
NATURAL & APPLIED SCIENCES
CIVIL ENGINEERING DEPARTMENT

Name of the Thesis: Stability Assessment of Seyrantepe Caves in Gaziantep

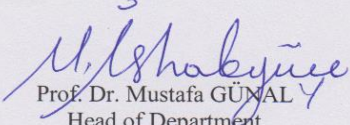
Name of the Student: Serdar ALLI

Exam Date: 06.06.2014


Approval of the Graduate School of Natural and Applied Sciences


Assoc. Prof. Dr. Metin BEDİR
Director

I certify that this thesis satisfies all there requirements as a thesis for the degree of Master of Science.


Prof. Dr. Mustafa GÜNAL
Head of Department

This is to certify that we have read this thesis and that in our opinion it is fully adequate, in scope and quality, as a thesis for the degree of Master of Science.


Assoc. Prof. Dr. Hanifi ÇANAKÇI
Supervisor

Examining Committee Members

Signature

Assoc. Prof. Dr. Hanifi ÇANAKÇI

Assist. Prof. Dr. Mehmet İshak YÜCE

Assist. Prof. Dr. Kasım MERMERDAŞ


.....
.....
.....

I hereby declare that all information in this document has been obtained and presented in accordance with academic rules and ethical conduct. I also declare that, as required by these rules and conduct, I have fully cited and referenced all material and results that are not original to this work.

Serdar ALLI

ABSTRACT

STABILITY ASSESSMENT OF SEYRANTEPE CAVES İN GAZİANTEP

ALLI, Serdar

M.Sc. in Civil Engineering.

Supervisor: Assoc. Prof. Dr. Hanifi ÇANAKÇI

June 2014, 82 pages

The collapse of caves due to excessive spans or insufficient rock cover is a major geotechnical hazard in rock masses that are prone to the stability problems. Analytical solutions for the stability of near surface caves in rock masses are rarely used because of the inherently discontinuous nature of the problem; instead, numerical approaches such as the finite element, discrete element, or hybrid methods of analysis are typically employed. In this thesis integrated experimental, analytical and numerical analyses were undertaken to assess the stability condition of Seyrantepe caves which were excavated into limestone. The sizes of the caves were measured in the field. Rock mass characterization was performed. The RMR, GSI and Q indexes were utilized for rock mass classification. A back analysis was performed on the recently collapsed section of the caves. The RocLab software based on Hoek-Brown failure criteria, and Mohr-Coulomb failure criteria were also used to determine the geotechnical parameters of the rock mass. The effects of the adjacent spans of the caves on the stability and failure zone were investigated. Back analysis results gave the lower strength parameters compared with Mohr Coulomb. RocLab results became on the safe side for this massive rock mass. The results showed that limit roof span was between 12 and 15 m for the roof thickness of 9 m and some countermeasures against instability were necessary.

Keywords: Caves; Stability; Back Analysis.

ÖZ

GAZİANTEP’TEKİ SEYRANTEPE MAĞARALARININ DURAYLILIĞININ DEĞERLENDİRİLMESİ

ALLI, Serdar
Yüksek Lisans Tezi, İnşaat Müh. Bölümü
Tez Yöneticisi: Doç Dr. Hanifi ÇANAKÇI
Haziran 2014, 82 sayfa

Geniş açıklığından ve yetersiz kaya örtüsünden dolayı mağaraların göçmesi duraysızlık problemlerine maruz kaya kütleleri içinde geoteknik açıdan incelenebilecek bir tehlikedir. Kaya kütleleri içinde sığ derinlikteki mağaraların duraylılığı için analitik çözümler kaya kütlelerinin doğal süreksizlikleri nedeniyle nadiren kullanılmaktadır. Bunun yerine, sonlu elemanlar, ayrık elemanlar ya da melez metotlar sıklıkla yapılmaktadır. Bu tezde, deneysel, analitik ve numerik analizler, kireçtaşı içinde açılmış olan Seyrantepe mağaralarının duraylılığını değerlendirmede beraberce ele alınmıştır. Mağaraların boyutları yerinde ölçülmüştür. Kaya kütle sınıflandırılması yapılmıştır. Kaya kütlelerinin sınıflandırılmasında RMR, GSI ve Q indekslerinden yararlanılmıştır. Mağaraların kısa zaman önce göçen kesiti üzerine geriye dönük analiz yapılmıştır. Hoek-Brown yenilme kriterine dayanan RocLab programı ve Mohr-Coulomb yenilme kriteri kaya kütlelerinin geoteknik parametrelerini hesaplamada ayrıca kullanılmıştır. Mağaraların komşu açıklığının duraylılık ve göçük alanı üzerindeki etkileri incelenmiştir. Geriye dönük analiz sonuçları Mohr-Coulomb’a kıyasla daha düşük dayanım parametreleri vermiştir. RocLab sonuçları bu masif kaya kütleleri için daha güvenli tarafta olmaktadır. Sonuçlar 9 m tavan kalınlığı için açıklığın genişliğinin 12 ila 15 m arasında olmasını ve duraysızlıklara karşı bazı koruyucu önlemlerin gerektiğini göstermiştir.

Anahtar Kelimeler: Mağaralar; Duraylılık; Geriye Dönük Analiz.

Sevgili Ablam Sema'ya...

ACKNOWLEDGEMENTS

I would like to express my sincere gratitude to my supervisor Assoc. Prof. Dr. Hanifi ÇANAKÇI for his invaluable guidance, advices, and supervision. It was my pleasure to work under his guidance.

I would like to express my sincere gratitude to Prof. Dr. Hasan Gerçek for his support. Without his support, this thesis would not have been completed.

I would also like to thanks to Gaziantep Metropolitan Municipality for the kind help.

I would like to special thanks to Civil Engineering Department of Bartın University for their support.

Finally my special thanks are reserved for my parents, all my family members. They have given me an endless enthusiasm and encouragement.

TABLE OF CONTENTS

	Page
ABSTRACT	v
ÖZ	vi
ACKNOWLEDGEMENTS	viii
TABLE OF CONTENTS	ix
LIST OF TABLES	xii
LIST OF FIGURES	xiii
CHAPTER 1	1
INTRODUCTION	1
1.1 General	1
1.2 Objective of Study	4
1.3 Organization of Study	4
CHAPTER 2	6
BACKGROUND	6
2.1 Literature Study	6
2.2 Limestone as a Rock	12
2.3 Rock Mass Classification Systems	13
2.3.1 Rock Mass Rating System (RMR)	14
2.3.2 Rock Tunnelling Quality Index, (Q)	17
2.3.3 Geological Strength Index (GSI)	20
2.4 Rock Mass Properties	22
2.4.1 Hoek-Brown Failure Criterion	22
2.4.2 Mohr Coulomb Failure Criterion	26

CHAPTER 3	29
SEYRANTEPE CAVES	29
3.1 Introduction	29
3.2 Geological Setting Of Seyrantepe Caves	33
3.3 Field Investigation.....	34
3.4 Determination of the Rock Mass Geotechnical Parameters.....	38
3.4.1 Experimental Studies	38
3.4.2 Determination of the Rock Mass Geotechnical Parameters with Hoek- Brown Criterion	39
3.4.3 Determination of the Rock Mass Geotechnical Parameters with Mohr- Coulomb Criterion	41
3.4.4 Back Analysis	42
CHAPTER 4	44
NUMERICAL ANALYSIS TO ASSESS THE STABILITY.....	44
4.1 Introduction	44
4.2 Finite Element Method with Plaxis Software	45
4.3 Modeling The Caves Using Plaxis Software	45
4.4 Results of Analysis.....	50
CHAPTER 5	58
EMPIRICAL APPROACHES TO ASSESS THE STABILITY	58
5.1 Assesment of the Stability with Rock Mass Classification Systems	58
CHAPTER 6	64
ANALYTICAL APPROACHES TO ASSESS THE STABILITY.....	64
6.1 Analysis by Euler Bernoulli Bending Theory	64
6.2 Analysis by Considering Shearing Stress together with Normal Stress	69
6.3 Pillar Analysis	72
CHAPTER 7	77

CONCLUSION AND RECOMMENDATIONS	77
REFERENCES	80

LIST OF TABLES

	Page
Table 2.1 Test results of Gaziantep limestone via genetic programming (Baykasoğlu et. al, 2007).....	13
Table 2.2 Given ratings to calculate the RMR (Hoek, E.).....	15
Table 2.3 Estimation of the support systems based on RMR (Hoek, E.).....	16
Table 2.4 Ratings of the parameters given in equation 2.1 to calculate the index Q (Hoek, E.).....	18
Table 2.4 (cont'd) Ratings of the parameters given in equation 2.1 to calculate the index Q (Hoek, E.).....	19
Table 2.5 The values of ESR (Hoek, E.).....	20
Table 2.6 Prediction of the value of D (Hoek et. al, 2002).....	24
Table 2.7 Prediction of the constant m_i (Hoek, E.).....	25
Table 2.8 Prediction of the σ_{ci} (Hoek, E.).....	26
Table 3.1 Laboratory test results performed on the core samples obtained from borings.....	39
Table 3.2 Geotechnical properties of Seyrantepe caves rock mass as determined by the tunnel application option of RocLab.....	40
Table 3.3 Calculated rock mass geotechnical parameters with Mohr-Coulomb criteria.....	42
Table 3.4 Geotechnical properties of rock mass based on back analysis.....	43
Table 4.1 Mechanical properties of briquette wall.....	50
Table 5.1 Description and illustrations of stability categories. (Aydan and Tokashiki 2011).....	61
Table 5.2 The values of a and b in Equation 5.1 and Equation 5.2 (Aydan and Tokashiki 2011).....	62
Table 6.1 Calculation table to determine the stress state in the cross section near the fixed support.....	72
Table 6.2 Most applicable of empirical strength formula for pillars (Karpuz and ...	75

LIST OF FIGURES

	Page
Figure 1.1 View of the partially collapsed cave named Üzümcü in Delbes Neighbourhood (Gaziantep Metropolitan Municipality)	2
Figure 1.2 Appearance of the collapsed cave in Çamlıca Neighbourhood (Gaziantep Metropolitan Municipality).....	3
Figure 1.3 Appearance of the sinkhole in Gaziantep Metropolitan Municipality Cemetery	3
Figure 1.4 Appearance of the collapsed cave in Kılınçoğlu Neighbourhood	4
Figure 2.1 Appearance of Little Palace and unstable rock block drawn by straight line. (Akgün and Koçkar, 2003).....	7
Figure 2.2 (a) The distribution of maximum principal stress, (b) the distribution of minimum principal stress, and (c) total displacements improved on the pillar thickness of 0.93 m between the caves. (Akgün and Koçkar, 2003). 8	8
Figure 2.3 (a) The distribution of maximum principal stress, (b) the distribution of minimum principal stress, and (c) total displacements improved on the pillar thickness of 0.10 m between the caves. (Akgun and Koçkar, 2003). 9	9
Figure 2.4 Boundaries between safe, marginal, and unsafe geometries for shallow caverns in blocky rock masses (Hatzor et. al, 2010).....	10
Figure 2.5 Inside view of the roof of Ayalon cave (Hatzor et. al, 2010)	11
Figure 2.6 Stress, strength contour and principal stresses for model F1 with the values of k_0 (Huang et. al, 2002)	12
Figure 2.7 The relationship between roof span and stand up time for the different RMR values (Hoek, E.).....	16
Figure 2.8 Estimation of the support systems based on index Q (Hoek, E.)	20
Figure 2.9 The values of GSI for different surface condition and structure of rock (Hoek, E.).....	21
Figure 2.10 Mohr Coulomb failure criterion	27

Figure 3.1 Location plan of the Seyrantepe caves	30
Figure 3.2 General view of Seyrantepe caves	31
Figure 3.3 Location and inner view of the top floor of Seyrantepe caves (photo: Gaziantep Metropolitan Municipality).....	32
Figure 3.4 Geological map of Gaziantep, scale: 1/100,000 (MTA, 1997).....	33
Figure 3.5. Horizontal bedding plane of Seyrantepe caves.....	34
Figure 3.6 Cracks observed in the roofs and rock pillars of the caves and alteration.	35
Figure 3.7 Shear failures of rock pillars observed along the section 1-1 of the caves and rock fall in cave no 5	36
Figure 3.8. General view of the cave no 5 before and after the rock fall.....	36
Figure 3.9. Location of the rock fall and shear failures of rock pillars along the section 1-1	37
Figure 3.10 Main window of RocLab software used for input and output data	41
Figure 4.1. General Classification of Numerical Methods	44
Figure 4.2 Dimesion of the caves along section 1-1	47
Figure 4.3 Finite element mesh and boundary conditions along section 1-1.....	48
Figure 4.4 Plastic points based on FEM analysis and failure zones observed in situ	52
Figure 4.5 Relative shear stresses	53
Figure 4.6 Total displacements	53
Figure 4.7 Vertical displacements.....	54
Figure 4.8 Horizontal displacements.....	54
Figure 4.9 Principal stresses.....	55
Figure 4.10 Axial forces in the wall.....	55
Figure 4.11 Shear forces in the wall.....	56
Figure 4.12 Bending moments in the wall	56
Figure 4.13 The failure zones around the cave no 7 without considering the adjacent caves.....	57
Figure 4.14 The failure zones around the cave no 7 with considering the adjacent caves.....	57
Figure 5.1 The relationship between roof span and stand up time for different RMR value of Seyrantepe caves	58
Figure 5.2 Estimated support categories based on the tunnelling quality index Q....	59

Figure 5.3 Comparison of empirical linear function for different stability categories with observations.	62
Figure 5.4 Comparison of empirical power function for different stability categories with observations.	63
Figure 5.5 Comparison of empirical functions proposed by Aydan and Tokashiki (2011) with functions of Barton.	63
Figure 6.1 Normal stresses based on Euler Bending Theory. a) Bending moment positive, b) Bending moment negative	65
Figure 6.2 Shear forces and bending moments for a flat roof of an underground space	66
Figure 6.3 Stability assessment chart of seyrantepe caves in terms of Euler Bernoulli Bending Theory.....	68
Figure 6.4 Shear forces and bending moments for the widest span of Seyrantepe caves.....	68
Figure 6.5 Normal stresses resulting from bending theory along the widest span of Seyrantepe caves	69
Figure 6.6 Shearing stress distribution of the rectangular beam.....	69
Figure 6.7 Principal stress of the rectangular beam	72
Figure 6.8 Bases of the tributary area method for estimating average axial pillar stress (Brady and Brown, 2004).....	74
Figure 6.9 Average pillar strength for different shaped pillars (Karpuz and Hindistan, 2008).	74

CHAPTER 1

INTRODUCTION

1.1 General

Gaziantep is a province located in the crossroads of the south eastern and mediterranean regions of Turkey, and ideally located to become a local industrial and commercial centre. The city is the most developed province in southeastern Turkey in terms of industrial and commercial activities. The population of the city keeps increasing due to being the center of attraction for the region. According to Address Based Population Registration System, TÜİK (Turkstat-Turkish Statistics Institute) is announced the population of Gaziantep is 1.844.438 at the the end of 2013 and increases 43.5 % compared to the year of 2000. The city is also in second place after Istanbul according to population growth rate between 2000 and 2010 in Turkey (TÜİK).

Limestone is a widespread rock type covering a large area in the city. By using this rock, houses were constructed in the past. Due to the easily available in the city and utilizing for building of the houses, the rock was carved to be used for house building until the middle of the 20th. century. Because of carving of the rock for the construction of stone houses, many underground spaces like caves having different sizes and shape were formed under the city (Çanakçı and Güllü, 2008).

The quick rise in the population of the province led to urban sprawls that various houses were built over these caves without considering any geotechnical investigation. Moreover much of them are still being utilized for working spaces like yarn, furniture production, storage spaces etc. It is known that many structures and streets are also underlain by the caves, but their places are not exactly known. The caves are commonly encountered by excavating for diverse construction works in the city. Unluckily, any remarkable study had not been performed to define the their places and numbers (Çanakçı, 2007).

The existence of these caves have potential hazards for the city. Some cave collapses were documented in the past. Recently, some new collapses were observed in the city. A cave named Üzümcü, located in Delbes neighbourhood partially collapsed on 14th of January, 2012. The collapse caused remarkable hazard to ten houses; collapsed three houses also injured one person (Figure 1.1). A cave located in Çamlıca neighbourhood, Nuripazarbaşı Street, collapsed on 30th of January, 2012. This collapse caused damaged to two shops (Figure 1.2). A cave located in Gaziantep Metropolitan Municipality Cemetery collapsed on 3th of February, 2012. This collapse caused to occurrence of a considerably wide sinkhole at the surface (Figure 1.3). After one day, a cave located in Kılınçoğlu neighbourhood, collapsed. It caused remarkable hazard to seven houses and collapsed one house (Figure 1.4). All of these disasters created widespread media area and disquieted among people.

Gaziantep is still carrying danger of recently collapses and disasters. People living around the caves has concerns against the collapse of them. Therefore, it is required to evaluate the stability of the caves correctly.



Figure 1.1 View of the partially collapsed cave named Üzümcü in Delbes Neighbourhood (Gaziantep Metropolitan Municipality)



Figure 1.2 Appearance of the collapsed cave in Çamlıca Neighbourhood (Gaziantep Metropolitan Municipality)



Figure 1.3 Appearance of the sinkhole in Gaziantep Metropolitan Municipality Cemetery



Figure 1.4 Appearance of the collapsed cave in Kılınçoğlu Neighbourhood

1.2 Objective of Study

In this study Seyrantepe caves in Gaziantep are discussed as an example. The main objective of the study is to perform stability assessment of the Seyrantepe caves. The purposes of this study are listed as follows:

- a) Analysis and evaluation of input parameters needed for stability assessment.
- b) Making the rock mass classification of caves.
- c) Evaluation rock mass properties of the caves.
- d) Stability assessment of Seyrantepe caves using numerical empirical and analytical methods.
- e) Investigation the effects of adjacent spans of the caves on the stability.
- f) Calculation the global factor of safety (FS) against failure.

1.3 Organization of Study

The thesis consists of seven chapters which are arranged as follows;

Chapter 1 includes a general view related to the study by considering the recent cave collapses in Gaziantep.

Chapter 2 includes the literature study related to stability of the caves, rock mass classification systems and rock mass properties.

Informations related to Seyrantepe caves such as, sizes, roof thicknesses, geological setting, field investigation etc. are given in chapter 3. Determination of the rock mass geotechnical parameters is also presented in this chapter.

Chapter 4 includes the numerical analysis to assess the stability. FEM analysis with plaxis software, modeling the caves using plaxis software, stability assessment based on back analysis results are presented in this chapter.

Chapter 5 includes the empirical methods to assess the stability. Approaches suggested by some researchers are discussed in this chapter.

Chapter 6 includes the analytical methods to assess the stability. Bending theory, analysis considering shearing stress and normal stresses, pillar analysis are discussed in this chapter.

The conclusion and recommendations drawn from study are given in chapter 7.

CHAPTER 2

BACKGROUND

2.1 Literature Study

Many studies are encountered in the scientific papers related to stability assessment of near surface caves. Some researchers focused on the failure mechanisms of cave while some researchers investigated the effects of cave shapes, sizes, roof thickness and pillars on the stability.

A case study was done by Akgün and Koçkar (2003). The study mainly focuses on presenting a method related to anchorage design and stability assessment of caves in silty sandstone limestone. The method was evaluated by examining the geomechanical conditions of the ancient Hasankeyf region. A dam namely Ilisu was suggested to be built over the area and Hasankeyf would remain under the water. In the study, It was stated that problem in the region comprised of the failure possibility of planar block which support one of the distinguished ancient structures, also rock falls from the roof of the caves excavated in the rock mass due to inadequate support thicknesses. Raising the water in dam reservoir, could speed up the failure of rock mass in the region that could cause to hazardous events for people who came to the ancient region which stayed over the maximum reservoir level. Firstly, the authors evaluated the geological condition and characterization of the rock mass for considering area. For rock mass characterization GSI and RMR methods were used. To determine the geotechnical properties RocLab was used for the assessment of the stability of the cave settlements.

For the first problem in the region, the authors discussed the Little Palace which is an significant ancient structure of Hasankeyf. This structure is under danger of kinematic failure throughout substantial crack observed in the rock mass under its foundation. Figure 2.1 shows view of Little Palace. Back analysis was performed to this kinematic failure block which support Little Palace to calculate the Mohr-Coulomb parameters which balance limit condition throughout the slip surface of the

rock block. To determine the Mohr Coulomb parameters a sensitivity analysis was also performed by considering water condition (wet, dry, fast drawdown conditions) and anticipated earthquake acceleration coefficient. According to their sensitivity analysis results, factor of safety against failure diminished with the smaller cohesion, greater frictional angle which balance limit condition. Authors also extended sensitivity analysis with unstable rock block by considering the water condition of the reservoir, anticipated earthquake acceleration coefficient and inclination angle of rock anchor. The sensitivity analysis results showed that for fast drawdown condition, minimum anchor force needed to stabilize the planar kinematic block.

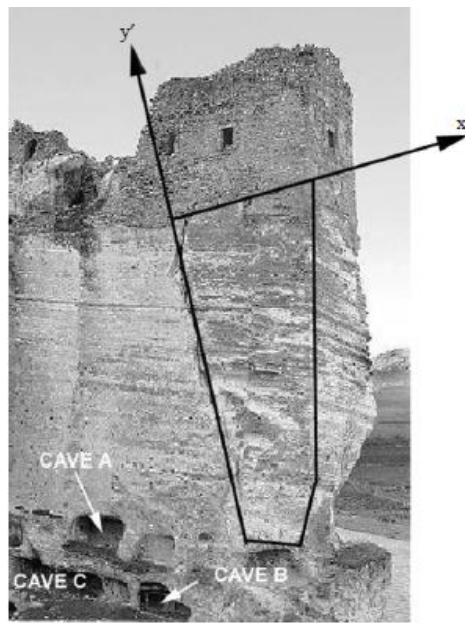


Figure 2.1 Appearance of Little Palace and unstable rock block drawn by straight line. (Akgün and Koçkar, 2003)

In the study, stresses and deformations around Cave B and C were determined. In addition required pillar thicknesses were calculated between Cave B and Cave C. Stability of the pillars were studied. Authors analyzed totally nine pillars having different thicknesses. These pillars ranged from 0.1 to 0.93 m. According to their results, pillars having the thickness between 0.1 and 0.2 m gave the roof collapse. Figure 2.2 and Figure 2.3 show the maximum and minimum principal stress conditions together with the total displacements for the pillars having the 0.93 m. and 0.10 m, respectively.

As seen in Figure 2.2 and Figure 2.3, tensile stresses and total displacements descend with ascending pillar thickness. As a result of this study, authors proposed to

implement a steel arch support between the caves rather than applying the wall having less or equal thickness of 0.5 m

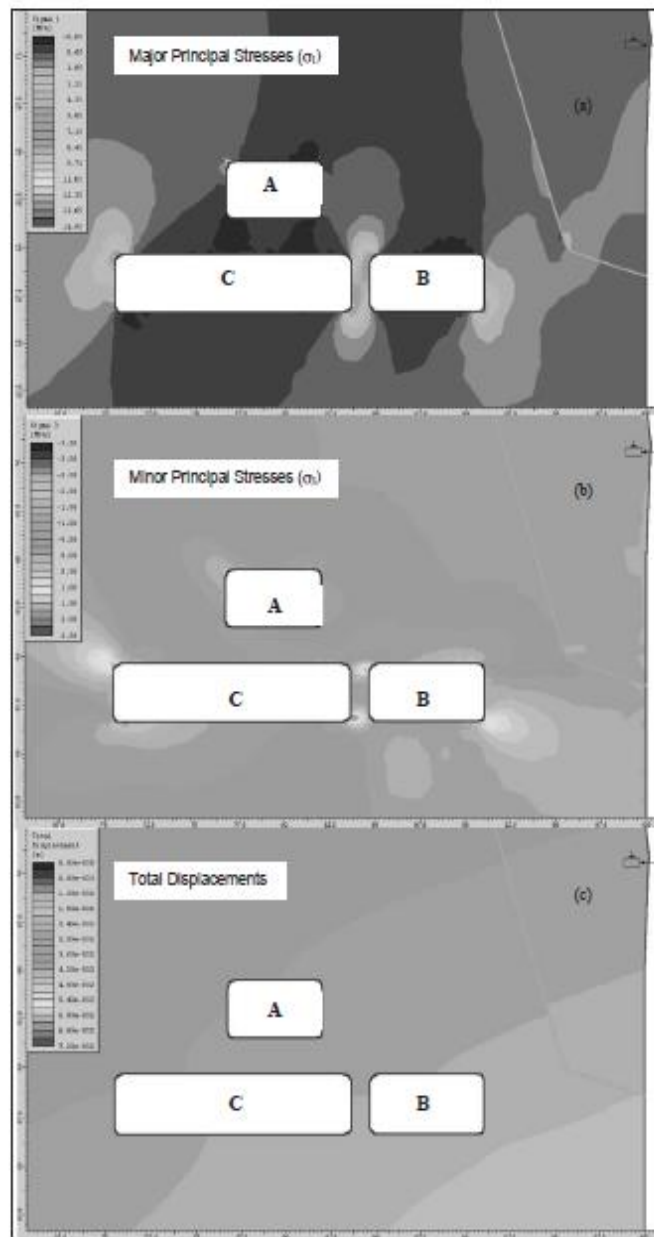


Figure 2.2 (a) The distribution of maximum principal stress, (b) the distribution of minimum principal stress, and (c) total displacements improved on the pillar thickness of 0.93 m between the caves. (Akgün and Koçkar, 2003)

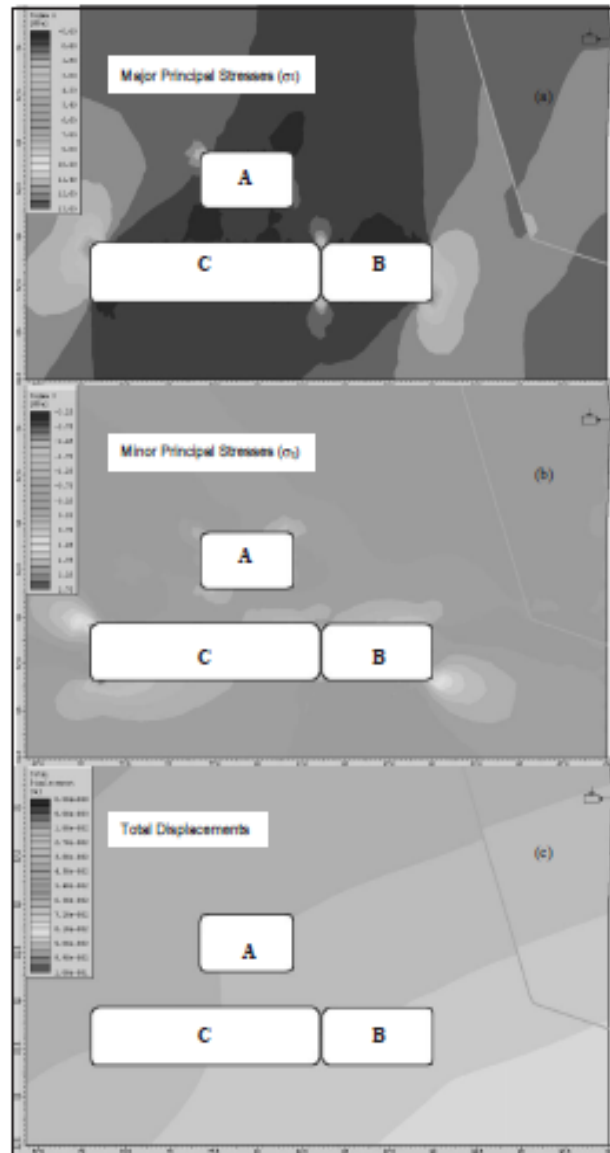


Figure 2.3 (a) The distribution of maximum principal stress, (b) the distribution of minimum principal stress, and (c) total displacements improved on the pillar thickness of 0.10 m between the caves. (Akgun and Koçkar, 2003)

One another study was carried out by Hatzor et. al (2010). They assessed the stability of shallow karstic caverns in blocky rock masses. Firstly authors performed numerical analysis using discontinuous deformation analysis known as DDA method for different sizes of the caverns. Totally, nineteen cavern sizes changed with spans and roof thickness were considered in their numerical analyses. Numerical analyses showed that stability is sufficient when the ratio of roof thickness to cavern span (h/B) is 0.33 up to cavern spans of 18 m. When the span is greater than 18 m, roof thickness swiftly increase and it seems to be stable at the ratio of $h/B=1.0$ for $h=26$ m and above (Figure 2.4).

Authors also analyzed some case studies to validate their numerical calculations. One of them is Ayalon cave. This cave has been located below an open pit mine in Israel and except for local roof collapse as seen in Figure 2.5, the cave is free standing. The roof cover of the cave is 30 m, the span is 40 m. The cave remains marginally stable according to their model estimation. Their model estimation was later validated considering two added studies in blocky rock masses. They have very different geotechnical parameters such as density, deformation modulus, intact rock strength. As a result of the study, authors stated that their model estimations is valid if the rock mass is in blocky category.

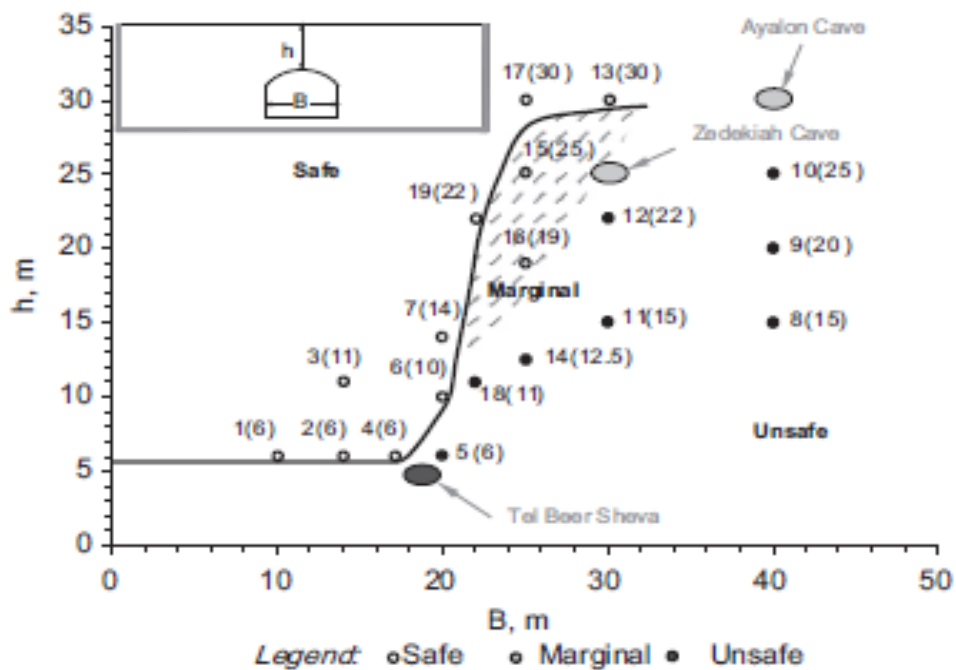


Figure 2.4 Boundaries between safe, marginal, and unsafe geometries for shallow caverns in blocky rock masses (Hatzor et. al, 2010)



Figure 2.5 Inside view of the roof of Ayalon cave (Hatzor et. al, 2010)

Huang et. al (2002) studied arching mechanism, the stability of the cavern roof and rockbolting. Authors evaluated the effects of usage different type of rockbolts on the stability. They also investigated the roof arching mechanism. Xiaolangdi powerhouse cavern was dealt with reinforcing its walls and roof. Tensioned cable anchors and fully grouted rock bolts with the arching theory were discussed by the authors. The effects of tensioned cable anchors and fully grouted rock bolts on the reinforcement were investigated by considering the arching theory.

Their results showed that when a natural and reinforced roof arch has been formed the extra tensioned cable can not be logical for the roof stability. The cables are not both safe and efficient because of inducing stress condition and the effect of the roof and wall displacement. Principal stress contours obtaining from numerical modeling is useful to establish and define the location and roof arch thickness (Figure 2.6). The authors also stated that to abstain from tensile stress and shearing along the joints in the roof, efforts should be made.

For the jointed rock, in reinforcement of the roof arch, the authors suggested to use closely spaced and short grouted rockbolts in case of tensioned cables.

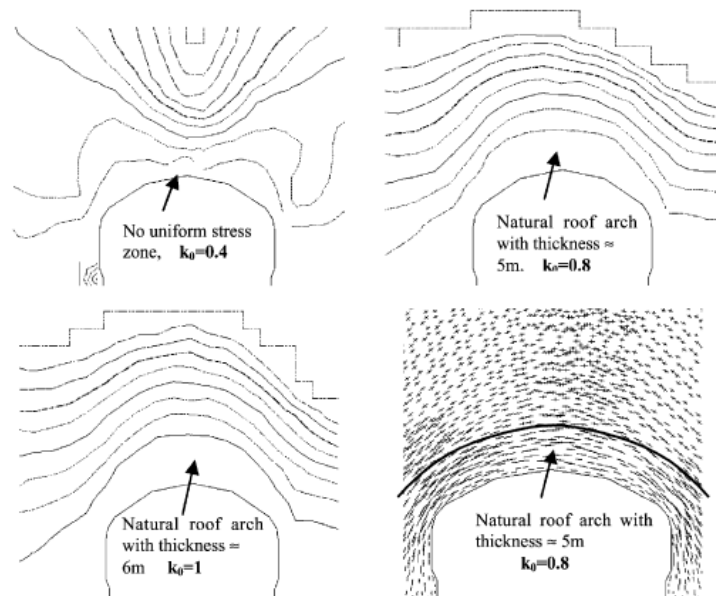


Figure 2.6 Stress, strength contour and principal stresses for model F1 with the values of k_0 (Huang et. al, 2002)

2.2 Limestone as a Rock

Rocks are the geological units formed by combining one or more minerals, or mineraloids and classified according to how they are formed. In terms of the formation, the rocks are classified under three rock types as metamorphic, igneous and sedimentary rocks.

Limestone is classified as sedimentary rock consisted of the minerals aragonite and calcite, which are distinct crystal form of calcium carbonate (CaCO_3). Mostly limestone formed from the accumulation of organisms on the bottom of the ocean, and usually extend over large areas. Some of these were later uplifted by tectonic forces in the earth and now exist below land areas. For example, much of Florida is underlain by this type limestone (Coduto et. al, 2010). Also, it is known that some limestones are formed exactly by chemical sedimentation of aragonite and calcite.

Limestone can be dissolved by long exposure to water, especially if it contains a mild solution of carbonic acid. Groundwater often gains small quantities of this acid through exposure to carbon dioxide in the ground. This process often produce karst topography, which exposes very ragged rock at the ground surface and many underground caves and passageways (Coduto et. al, 2010).

Geotechnical properties of limestone provide input data to determine the stability of caves. The prediction of tensile and uniaxial compressive strength of limestone in Gaziantep was studied by Baykasoğlu et. al (2007) via genetic programming. Bulk density, saturated density, water absorption, ultrasonic pulse velocity and dry density were used as input datas in the genetic programming techniques of the authors. Moreover, two main strength properties, tensile strength and uniaxial compressive strength were calculated as the output datas. According to their study the uniaxial compressive strength (UCS) of Gaziantep limestone is found as between 3.7 MPa and 67.4 MPa and the average value is 10.7 MPa. Standard deviation is 9.6. The strength of limestone can be classified as weak rock to very weak rock according to ISRM (1981). By brazilian method, tensile strengthes are calculated as between 1.0 MPa and 15.1 MPa and the average value is 3.8 MPa. Standard deviation is 2.5. Table 2.1 presents Gaziantep limestone's test results.

Table 2.1 Test results of Gaziantep limestone via genetic programming (Baykasoğlu et. al, 2007)

Sample set	Test	Minimum	Maximum	Mean	STD
Sample set 1 (total sample = 106)	UCS (MPa)	3.7	67.4	10.7	9.6
	UPV (m/s)	2041	5735	2637	751
	Water absorption (%)	1	27	18	6
	Dry density (g/cm ³)	1.42	2.54	1.73	0.25
	Saturated density (g/cm ³)	1.81	2.57	2.02	0.18
	Bulk density (g/cm ³)	1.42	2.62	1.72	0.25
Sample set 2 (total sample = 118)	Tensile strength (MPa)	1.0	15.1	3.8	2.5
	UPV (m/s)	1947	5909	3380	1214
	Water absorption (%)	2	25	13	7
	Dry density (g/cm ³)	1.46	2.62	1.91	0.34
	Saturated density (g/cm ³)	1.82	2.66	2.14	0.24
	Bulk density (g/cm ³)	1.18	2.59	1.90	0.35

2.3 Rock Mass Classification Systems

Rock has different properties compared with the most other engineering materials. It is not a homogeneous material in fact. It can consist fractures or some discontinuities such as faults, folds, bedding planes, joints. These structural features effect the mechanical properties of the rock medium in situ. That is, test results obtained for laboratory core samples are different those of performed for the rock mass in situ. Laboratory core samples are evaluated as intact rock. Thus an explicit difference must be between the rock mass and intact rock. Intact rock is the term used to define the rock medium between discontinuities. It can be represented by a piece of drill core or a hand specimen. The rock mass is the in situ environment including faults, bedding planes, folds, joints and other structural features.

Stability of rock mass is solely depends upon the rock mass quality and mechanical processes involve in it. Major input variables to identify quality of rock mass are rock mass strength, rock mass deformability, strength, anisotropy, discontinuity, weathering, and alteration. The stability of an underground excavation is interdependent with the structural condition in the rock mass, degree of weathering of the rock mass and their relationship between rock mass strength and rock stresses (Hoek and Brown, 1980).

The rock mass classification systems represent the rock mass quality. They can provide deformation and strength properties of the rock mass, primary estimates of support requirements. Some significant rock mass classification systems such as Q, RMR and GSI were taken into account in this thesis to assessment of the Seyrantepe caves and to determine the strength of the rock mass by using intact rock properties.

2.3.1 Rock Mass Rating System (RMR)

Rock mass rating system called the geomechanics classification system was developed by Barton (1973). During the past years, RMR system has been consecutively evolved. The RMR system involves the following parameters to classify a rock mass. These parameters are obtained from borings and measured in the field.

- a) Spacing of discontinuities
- b) Uniaxial compressive strength for intact rock
- c) Groundwater conditions
- d) Condition of discontinuities
- e) RQD
- f) Orientation of discontinuities

Table 2.2 presents the RMR system. Each of the parameters given above has the ratings. To calculate the value of RMR, these ratings are summed.

Bieniawski (1989) presented a method for the estimation of support in tunnels according to value of RMR (Table 2.3). In additions, Figure 2.7 shows the relationship between roof span and stand up time for the different RMR values.

When excavation of the caves, the RMR of Gaziantep Seyrantepe caves should be greater than 80 due to keeping their integrity for a long time with a 38,5 m maximum roof span. So the average RMR value of Seyrantepe caves is considered as 85 in this thesis. Rock mass class is in very good rock category.

Table 2.2 Given ratings to calculate the RMR (Hoek, E.)

A. CLASSIFICATION PARAMETERS AND THEIR RATINGS								
Parameter		Range of values						
1	Strength of intact rock material	Point-load strength index	>10 MPa	4 - 10 MPa	2 - 4 MPa	1 - 2 MPa	For this low range - uniaxial compressive test is preferred	
		Uniaxial comp. strength	>250 MPa	100 - 250 MPa	50 - 100 MPa	25 - 50 MPa	5 - 25 MPa	1 - 5 MPa
	Rating	15	12	7	4	2	1	0
2	Drill core Quality <i>RQD</i>	90% - 100%	75% - 90%	50% - 75%	25% - 50%	< 25%		
	Rating	20	17	13	8	3		
3	Spacing of discontinuities	> 2 m	0.6 - 2 . m	200 - 600 mm	60 - 200 mm	< 60 mm		
	Rating	20	15	10	8	5		
4	Condition of discontinuities (See E)	Very rough surfaces	Slightly rough surfaces	Slightly rough surfaces	Slickensided surfaces	Soft gouge >5 mm thick or Separation > 5 mm		
		Not continuous	Separation < 1 mm	Separation < 1 mm	or Gouge < 5 mm thick or Separation 1-5 mm	Continuous		
5	Groundwater	Inflow per 10 m tunnel length (l/m)	None	< 10	10 - 25	25 - 125	> 125	
		(Joint water press) / (Major principal σ)	0	< 0.1	0.1, - 0.2	0.2 - 0.5	> 0.5	
6	General conditions	Completely dry	Damp	Wet	Dripping	Flowing		
		Rating	15	10	7	4	0	
B. RATING ADJUSTMENT FOR DISCONTINUITY ORIENTATIONS (See F)								
Strike and dip orientations		Very favourable	Favourable	Fair	Unfavourable	Very Unfavourable		
Ratings	Tunnels & mines	0	-2	-5	-10	-12		
	Foundations	0	-2	-7	-15	-25		
	Slopes	0	-5	-25	-50			
C. ROCK MASS CLASSES DETERMINED FROM TOTAL RATINGS								
Rating	100 ← 81	80 ← 61	60 ← 41	40 ← 21	< 21			
Class number	I	II	III	IV	V			
Description	Very good rock	Good rock	Fair rock	Poor rock	Very poor rock			
D. MEANING OF ROCK CLASSES								
Class number	I	II	III	IV	V			
Average stand-up time	20 yrs for 15 m span	1 year for 10 m span	1 week for 5 m span	10 hrs for 2.5 m span	30 min for 1 m span			
Cohesion of rock mass (kPa)	> 400	300 - 400	200 - 300	100 - 200	< 100			
Friction angle of rock mass (deg)	> 45	35 - 45	25 - 35	15 - 25	< 15			
E. GUIDELINES FOR CLASSIFICATION OF DISCONTINUITY CONDITIONS								
Discontinuity length (persistence)	< 1 m	1 - 3 m	3 - 10 m	10 - 20 m	> 20 m			
Rating	6	4	2	1	0			
Separation (aperture)	None	< 0.1 mm	0.1 - 1.0 mm	1 - 5 mm	> 5 mm			
Rating	6	5	4	1	0			
Roughness	Very rough	Rough	Slightly rough	Smooth	Slickensided			
Rating	6	5	3	1	0			
Infilling (gouge)	None	Hard filling < 5 mm	Hard filling > 5 mm	Soft filling < 5 mm	Soft filling > 5 mm			
Rating	6	4	2	2	0			
Weathering	Unweathered	Slightly weathered	Moderately weathered	Highly weathered	Decomposed			
Rating	6	5	3	1	0			
F. EFFECT OF DISCONTINUITY STRIKE AND DIP ORIENTATION IN TUNNELLING**								
Strike perpendicular to tunnel axis				Strike parallel to tunnel axis				
Drive with dip - Dip 45 - 90°		Drive with dip - Dip 20 - 45°		Dip 45 - 90°		Dip 20 - 45°		
Very favourable		Favourable		Very unfavourable		Fair		
Drive against dip - Dip 45-90°		Drive against dip - Dip 20-45°		Dip 0-20 - Irrespective of strike°				
Fair		Unfavourable		Fair				

* Some conditions are mutually exclusive . For example, if infilling is present, the roughness of the surface will be overshadowed by the influence of the gouge. In such cases use A.4 directly.

** Modified after Wickham et al (1972).

Table 2.3 Estimation of the support systems based on RMR (Hoek, E.)

Rock mass class	Excavation	Rock bolts (20 mm diameter, fully grouted)	Shotcrete	Steel sets
I - Very good rock <i>RMR</i> : 81-100	Full face, 3 m advance.	Generally no support required except spot bolting.		
II - Good rock <i>RMR</i> : 61-80	Full face , 1-1.5 m advance. Complete support 20 m from face.	Locally, bolts in crown 3 m long, spaced 2.5 m with occasional wire mesh.	50 mm in crown where required.	None.
III - Fair rock <i>RMR</i> : 41-60	Top heading and bench 1.5-3 m advance in top heading. Commence support after each blast. Complete support 10 m from face.	Systematic bolts 4 m long, spaced 1.5 - 2 m in crown and walls with wire mesh in crown.	50-100 mm in crown and 30 mm in sides.	None.
IV - Poor rock <i>RMR</i> : 21-40	Top heading and bench 1.0-1.5 m advance in top heading. Install support concurrently with excavation, 10 m from face.	Systematic bolts 4-5 m long, spaced 1-1.5 m in crown and walls with wire mesh.	100-150 mm in crown and 100 mm in sides.	Light to medium ribs spaced 1.5 m where required.
V - Very poor rock <i>RMR</i> : < 20	Multiple drifts 0.5-1.5 m advance in top heading. Install support concurrently with excavation. Shotcrete as soon as possible after blasting.	Systematic bolts 5-6 m long, spaced 1-1.5 m in crown and walls with wire mesh. Bolt invert.	150-200 mm in crown, 150 mm in sides, and 50 mm on face.	Medium to heavy ribs spaced 0.75 m with steel lagging and forepoling if required. Close invert.

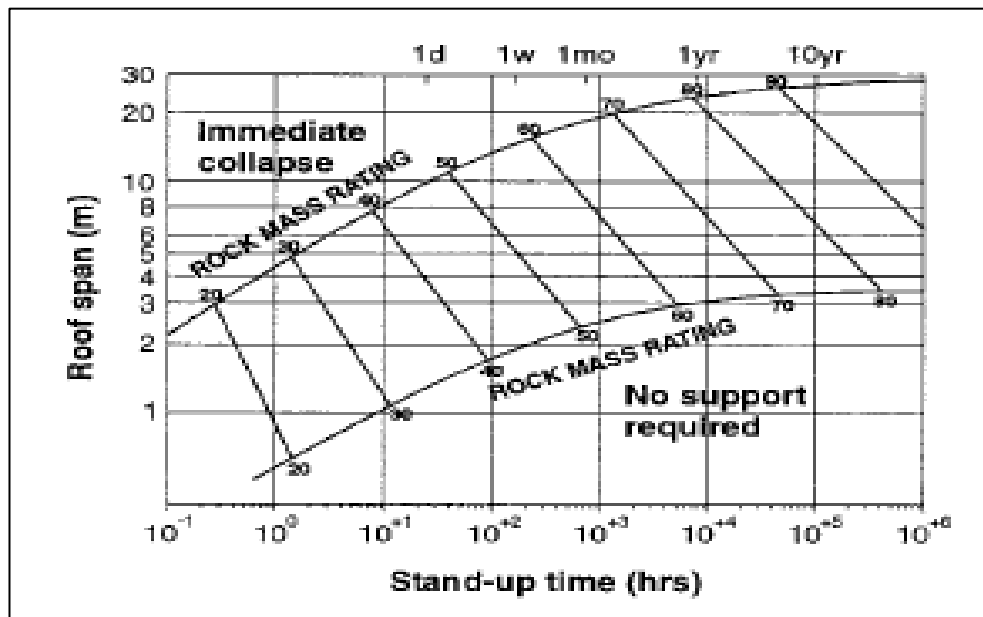


Figure 2.7 The relationship between roof span and stand up time for the different RMR values (Hoek, E.)

2.3.2 Rock Tunnelling Quality Index, (Q)

Barton et. al (1974) developed this classification to determine support requirements for tunnels and the rock mass quality. The value of Q varies from 0.001 to 1000 on a logarithmic scale. Q is determined by following equation.

$$Q = \left(\frac{RQD}{J_n} \right) \times \left(\frac{J_r}{J_a} \right) \times \left(\frac{J_w}{SRF} \right) \quad (2.1)$$

The parameters given above equation are presented in (Table 2.4). Each of the parameters has the ratings. To calculate the index Q, these ratings are summed. Figure 2.8 shows the support requirements for underground spans according to the index Q. The value of excavation support ratio (ESR) concerns with the planned use of the span and the level of security expected of the support system established to keep the stability of the span. Barton et. al (1974) propose the values of ESR in Table 2.5.

If the value of RMR is known, it is also possible to calculate the tunnelling quality index Q from following equation suggested by Bieniawski (1989).

$$RMR = 9 \ln Q + 44$$

By using the above relationship, value of Q is found as 54.6 for the RMR of 80, and 165.8 for the RMR of 90. Q is calculated as 95.2 with the average predicted RMR for Seyrantepe caves. Rock mass class is between very good and extremely good categories. These values have been used for further calculation.

Table 2.4 Ratings of the parameters given in equation 2.1 to calculate the index Q (Hoek, E.)

DESCRIPTION	VALUE	NOTES
1. ROCK QUALITY DESIGNATION	<i>RQD</i>	
A. Very poor	0 - 25	1. Where <i>RQD</i> is reported or measured as ≤ 10 (including 0), a nominal value of 10 is used to evaluate <i>Q</i> .
B. Poor	25 - 50	
C. Fair	50 - 75	
D. Good	75 - 90	2. <i>RQD</i> intervals of 5, i.e. 100, 95, 90 etc. are sufficiently accurate.
E. Excellent	90 - 100	
2. JOINT SET NUMBER	J_n	
A. Massive, no or few joints	0.5 - 1.0	
B. One joint set	2	
C. One joint set plus random	3	
D. Two joint sets	4	
E. Two joint sets plus random	6	
F. Three joint sets	9	1. For intersections use $(3.0 \times J_n)$
G. Three joint sets plus random	12	
H. Four or more joint sets, random, heavily jointed, 'sugar cube', etc.	15	2. For portals use $(2.0 \times J_n)$
J. Crushed rock, earthlike	20	
3. JOINT ROUGHNESS NUMBER	J_r	
<i>a. Rock wall contact</i>		
<i>b. Rock wall contact before 10 cm shear</i>		
A. Discontinuous joints	4	
B. Rough and irregular, undulating	3	
C. Smooth undulating	2	
D. Slickensided undulating	1.5	1. Add 1.0 if the mean spacing of the relevant joint set is greater than 3 m.
E. Rough or irregular, planar	1.5	
F. Smooth, planar	1.0	
G. Slickensided, planar	0.5	2. $J_r = 0.5$ can be used for planar, slickensided joints having lineations, provided that the lineations are oriented for minimum strength.
<i>c. No rock wall contact when sheared</i>		
H. Zones containing clay minerals thick enough to prevent rock wall contact	1.0 (nominal)	
J. Sandy, gravely or crushed zone thick enough to prevent rock wall contact	1.0 (nominal)	
4. JOINT ALTERATION NUMBER	J_a	ϕ_r degrees (approx.)
<i>a. Rock wall contact</i>		
A. Tightly healed, hard, non-softening, impermeable filling	0.75	1. Values of ϕ_r , the residual friction angle, are intended as an approximate guide to the mineralogical properties of the alteration products, if present.
B. Unaltered joint walls, surface staining only	1.0	25 - 35
C. Slightly altered joint walls, non-softening mineral coatings, sandy particles, clay-free disintegrated rock, etc.	2.0	25 - 30
D. Silty-, or sandy-clay coatings, small clay-fraction (non-softening)	3.0	20 - 25
E. Softening or low-friction clay mineral coatings, i.e. kaolinite, mica. Also chlorite, talc, gypsum and graphite etc., and small quantities of swelling clays. (Discontinuous coatings, 1 - 2 mm or less)	4.0	8 - 16

Table 2.4 (cont'd) Ratings of the parameters given in equation 2.1 to calculate the index Q (Hoek, E.)

4. JOINT ALTERATION NUMBER	J_a	ϕ degrees (approx.)	
<i>b. Rock wall contact before 10 cm shear</i>			
F. Sandy particles, clay-free, disintegrating rock etc.	4.0	25 - 30	
G. Strongly over-consolidated, non-softening clay mineral fillings (continuous < 5 mm thick)	6.0	16 - 24	
H. Medium or low over-consolidation, softening clay mineral fillings (continuous < 5 mm thick)	8.0	12 - 16	
J. Swelling clay fillings, i.e. montmorillonite, (continuous < 5 mm thick). Values of J_a depend on percent of swelling clay-size particles, and access to water.	8.0 - 12.0	6 - 12	
<i>c. No rock wall contact when sheared</i>			
K. Zones or bands of disintegrated or crushed	6.0		
L. rock and clay (see G, H and J for clay	8.0		
M. conditions)	8.0 - 12.0	6 - 24	
N. Zones or bands of silty- or sandy-clay, small clay fraction, non-softening	5.0		
O. Thick continuous zones or bands of clay	10.0 - 13.0		
P. & R. (see G.H and J for clay conditions)	6.0 - 24.0		
5. JOINT WATER REDUCTION	J_w	approx. water pressure (kgf/cm ²)	
A. Dry excavation or minor inflow i.e. < 5 l/m locally	1.0	< 1.0	
B. Medium inflow or pressure, occasional outwash of joint fillings	0.66	1.0 - 2.5	
C. Large inflow or high pressure in competent rock with unfilled joints	0.5	2.5 - 10.0	1. Factors C to F are crude estimates; increase J_w if drainage installed.
D. Large inflow or high pressure	0.33	2.5 - 10.0	
E. Exceptionally high inflow or pressure at blasting, decaying with time	0.2 - 0.1	> 10	2. Special problems caused by ice formation are not considered.
F. Exceptionally high inflow or pressure	0.1 - 0.05	> 10	
6. STRESS REDUCTION FACTOR		SRF	
<i>a. Weakness zones intersecting excavation, which may cause loosening of rock mass when tunnel is excavated</i>			
A. Multiple occurrences of weakness zones containing clay or chemically disintegrated rock, very loose surrounding rock any depth)		10.0	1. Reduce these values of SRF by 25 - 50% but only if the relevant shear zones influence do not intersect the excavation
B. Single weakness zones containing clay, or chemically disintegrated rock (excavation depth < 50 m)		5.0	
C. Single weakness zones containing clay, or chemically disintegrated rock (excavation depth > 50 m)		2.5	
D. Multiple shear zones in competent rock (clay free), loose surrounding rock (any depth)		7.5	
E. Single shear zone in competent rock (clay free). (depth of excavation < 50 m)		5.0	
F. Single shear zone in competent rock (clay free). (depth of excavation > 50 m)		2.5	
G. Loose open joints, heavily jointed or 'sugar cube', (any depth)		5.0	
6. STRESS REDUCTION FACTOR		SRF	
<i>b. Competent rock, rock stress problems</i>			
	σ_c/σ_1	σ_t/σ_1	
H. Low stress, near surface	> 200	> 13	2.5
J. Medium stress	200 - 10	13 - 0.66	1.0
K. High stress, very tight structure (usually favourable to stability, may be unfavourable to wall stability)	10 - 5	0.66 - 0.33	0.5 - 2
L. Mild rockburst (massive rock)	5 - 2.5	0.33 - 0.16	5 - 10
M. Heavy rockburst (massive rock)	< 2.5	< 0.16	10 - 20
<i>c. Squeezing rock, plastic flow of incompetent rock under influence of high rock pressure</i>			
N. Mild squeezing rock pressure			5 - 10
O. Heavy squeezing rock pressure			10 - 20
<i>d. Swelling rock, chemical swelling activity depending on presence of water</i>			
P. Mild swelling rock pressure			5 - 10
R. Heavy swelling rock pressure			10 - 15

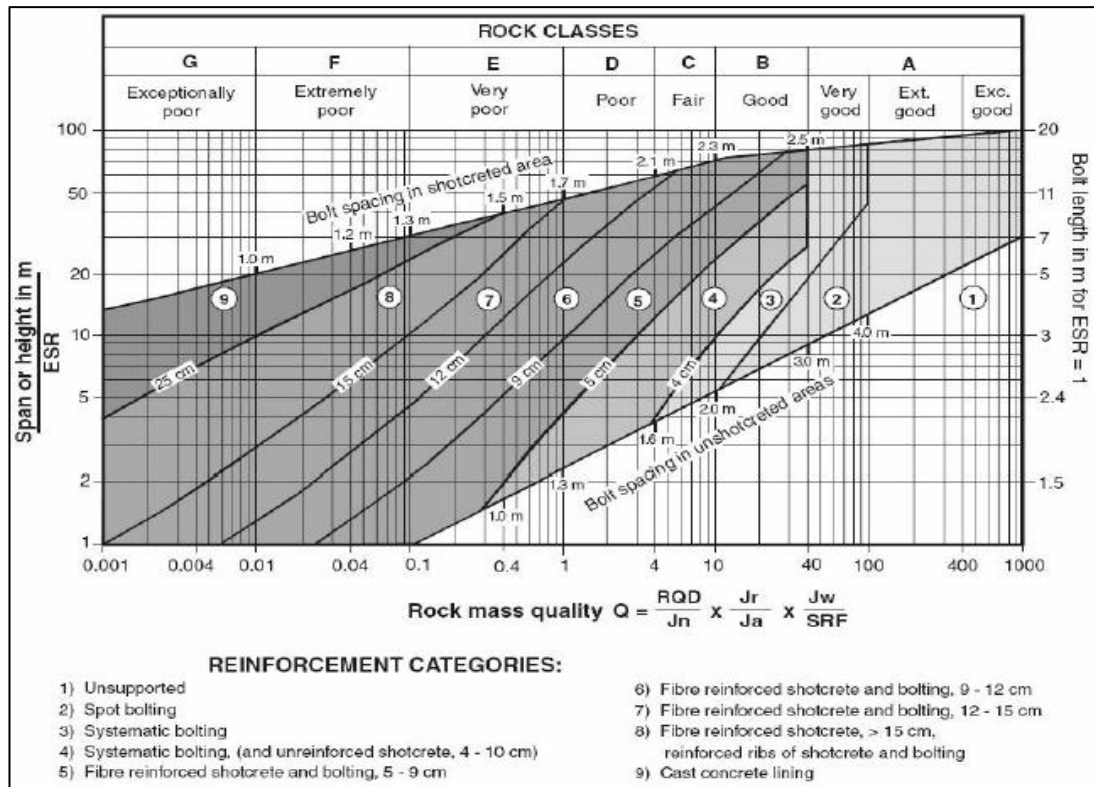


Figure 2.8 Estimation of the support systems based on index Q (Hoek, E.)

Table 2.5 The values of ESR (Hoek, E.)

Excavation category	<i>ESR</i>
A Temporary mine openings.	3-5
B Permanent mine openings, water tunnels for hydro power (excluding high pressure penstocks), pilot tunnels, drifts and headings for large excavations.	1.6
C Storage rooms, water treatment plants, minor road and railway tunnels, surge chambers, access tunnels.	1.3
D Power stations, major road and railway tunnels, civil defence chambers, portal intersections.	1.0
E Underground nuclear power stations, railway stations, sports and public facilities, factories.	0.8

2.3.3 Geological Strength Index (GSI)

The strength of a jointed rock mass depends on the properties of the intact pieces of rock and upon the freedom of those pieces to slide and rotate under a range of imposed stress conditions. This freedom is controlled by the shapes of the intact rock pieces as well as by the condition of the surfaces separating them.

Hoek (1994) and Hoek et. al (1995) introduced a new rock mass classification system known as the Geological Strength Index (GSI) to consider these two features

of the rock mass, its structure as represented by its blockiness and degree or interlocking, and the condition of the discontinuity surfaces. Then, the GSI was developed to overcome some of the deficiencies that had been identified in using the RMR system with the rock mass strength criterion (Hoek and Marinos, 2000).

The Geological Strength Index (GSI) provides a number which is used for estimating the reduction in rock mass strength for different geological conditions. The value of GSI may be estimated from visual exposures of the rock mass or borehole core by using Figure 2.9.

Before the excavation of the Seyrantepe caves, rock mass is evaluated as massive type with few widely spaced discontinuities. Surface of rock mass is very rough and fresh unweathered. Therefore, The value of GSI is estimated as greater than 80 in that time. For further analysis of caves, average GSI value of rock mass is considered as 85.

GEOLOGICAL STRENGTH INDEX FOR JOINTED ROCKS (Hoek and Marinos, 2000)		SURFACE CONDITIONS			
<p>From the lithology, structure and surface conditions of the discontinuities, estimate the average value of GSI. Do not try to be too precise. Quoting a range from 33 to 37 is more realistic than stating that GSI = 35. <u>Note that the table does not apply to structurally controlled failures.</u> Where weak planar structural planes are present in an unfavourable orientation with respect to the excavation face, these will dominate the rock mass behaviour. The shear strength of surfaces in rocks that are prone to deterioration as a result of changes in moisture content will be reduced if water is present. When working with rocks in the fair to very poor categories, a shift to the right may be made for wet conditions. Water pressure is dealt with by effective stress analysis.</p>		SURFACE CONDITIONS			
		VERY GOOD	GOOD	FAIR	POOR
STRUCTURE		DECREASING SURFACE QUALITY			
		VERY rough, fresh unweathered surfaces	Rough, slightly weathered, iron stained surfaces	Smooth, moderately weathered and altered surfaces	Slickensided, highly weathered surfaces with compact coatings or fillings or angular fragments
		SURFACE QUALITY			
		VERY POOR			VERY POOR
		Slickensided, highly weathered surfaces with soft clay coatings or fillings			
STRUCTURE		DECREASING SURFACE QUALITY			
INTACT OR MASSIVE - intact rock specimens or massive in situ rock with few widely spaced discontinuities		90			N/A
BLOCKY - well interlocked undisturbed rock mass consisting of cubical blocks formed by three intersecting discontinuity sets		80	70		
VERY BLOCKY- interlocked, partially disturbed mass with multi-faceted angular blocks formed by 4 or more joint sets			60		
BLOCKY/DISTURBED/SEAMY - folded with angular blocks formed by many intersecting discontinuity sets. Persistence of bedding planes or schistosity				50	
DISINTEGRATED - poorly interlocked, heavily broken rock mass with mixture of angular and rounded rock pieces				40	
LAMINATED/SHEARED - Lack of blockiness due to close spacing of weak schistosity or shear planes				30	
				20	
				10	
		N/A	N/A		

Figure 2.9 The values of GSI for different surface condition and structure of rock (Hoek, E.)

2.4 Rock Mass Properties

Deformation and strength characteristics of rock masses are very important to estimate the stability of underground spaces. These properties are controlled by the discontinuities and features of intact rock. Under this title, Hoek –Brown and Mohr Coulomb failure criteria are discussed to predict the deformation and strength characteristics of rock masses.

2.4.1 Hoek-Brown Failure Criterion

Correct calculation of the deformation and strength parameters of rock masses are very important for all analysis used for the design of foundation, slopes and underground spans. Hoek and Brown (1980a, 1980b) suggested a solution for calculating of the strength of the jointed rock masses according to the interlocking of rock blocks and the situation of the surfaces around these blocks. This solution was extended during the past years for meeting the requirements of the users related to the other rock mass classes and quality. For poor quality rock masses, a new classification system namely Geological Strength Index (GSI) was developed to calculate the deformation and strength parameters. A remarkable revision was performed in 2002 for the implementation of the criterion in numerical analysis and calculating Mohr Coulomb parameters. Prediction of the deformation modulus was made by Hoek and Diederichs (2006).

Following equation defines the Generalised Hoek-Brown failure criterion:

$$\sigma_1' = \sigma_3' + \sigma_{ci} \left(m_b \frac{\sigma_3'}{\sigma_{ci}} + s \right)^a$$

Where,

s and a are constants,

m_b is the value of the Hoek-Brown constant m for the rock mass,

σ_{ci} is the uniaxial compressive strength for intact rock sample,

σ_1' and σ_3' show the maximum and minimum effective principal stresses at failure.

The constants of a, s and m_b can be calculated by using the following equations

$$a = \frac{1}{2} + \frac{1}{6} \left(e^{-GSI/15} - e^{-20/3} \right)$$

$$s = \exp\left(\frac{\text{GSI}-100}{9-3D}\right)$$

$$m_b = m_i \exp\left(\frac{\text{GSI}-100}{28-14D}\right)$$

GSI is the geological strength index of rock mass that can be calculated in Figure 2.9. D is a number that shows the level of disturbance because of stress relaxation and blast. The value of D can be obtained from Table 2.6 for different rock masses and blast conditions. The values of m_i and σ_{ci} are calculated by triaxial compression tests on core sample. Table 2.7 and Table 2.8 can be used to predict the values of m_i and σ_{ci} if there are no laboratory results. The more detailed information can be available from Hoek and Brown (1997).

Therefore, three parameters of the rock are used to predict the deformability and strength in terms of Hoek Brown criterion. These are:

- GSI
- m_i , and
- σ_{ci}

It is possible to calculate Mohr Coulomb parameters by using above parameters. The transformation equations are presented in Hoek et. al (2002). These calculations can be also easily performed by the RocLab software.

For Gaziantep Seyrantepe caves, Hoek-Brown failure criterion was utilized to calculate the equivalent Mohr-Coulomb parameters, rock mass strength and deformation modulus by using the program RocLab. Later, obtained parameters were compared with those of back analysis. Determination of the rock mass strength and Hoek-Brown failure criterion parameters is presented in Chapter 3.

Table 2.6 Prediction of the value of D (Hoek et. al, 2002)




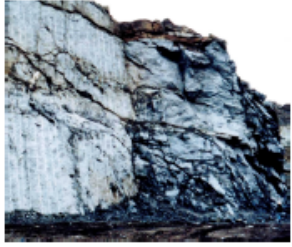

Appearance of rock mass	Description of rock mass	Suggested value of D
	Excellent quality controlled blasting or excavation by Tunnel Boring Machine results in minimal disturbance to the confined rock mass surrounding a tunnel.	D = 0
	Mechanical or hand excavation in poor quality rock masses (no blasting) results in minimal disturbance to the surrounding rock mass. Where squeezing problems result in significant floor heave, disturbance can be severe unless a temporary invert, as shown in the photograph, is placed.	D = 0 D = 0.5 No invert
	Very poor quality blasting in a hard rock tunnel results in severe local damage, extending 2 or 3 m, in the surrounding rock mass.	D = 0.8
	Small scale blasting in civil engineering slopes results in modest rock mass damage, particularly if controlled blasting is used as shown on the left hand side of the photograph. However, stress relief results in some disturbance.	D = 0.7 Good blasting D = 1.0 Poor blasting
	Very large open pit mine slopes suffer significant disturbance due to heavy production blasting and also due to stress relief from overburden removal. In some softer rocks excavation can be carried out by ripping and dozing and the degree of damage to the slopes is less.	D = 1.0 Production blasting D = 0.7 Mechanical excavation

Table 2.7 Prediction of the constant m_i (Hoek, E.)

Rock type	Class	Group	Texture			
			Coarse	Medium	Fine	Very fine
SEDIMENTARY	Clastic		Conglomerates* (21 ± 3)	Sandstones 17 ± 4	Siltstones 7 ± 2	Claystones 4 ± 2
			Breccias (19 ± 5)		Greywackes (18 ± 3)	Shales (6 ± 2) Marls (7 ± 2)
	Non-Clastic	Carbonates	Crystalline Limestone (12 ± 3)	Sparitic Limestones (10 ± 2)	Micritic Limestones (9 ± 2)	Dolomites (9 ± 3)
		Evaporites		Gypsum 8 ± 2	Anhydrite 12 ± 2	
Organic					Chalk 7 ± 2	
METAMORPHIC	Non Foliated		Marble 9 ± 3	Hornfels (19 ± 4) Metasandstone (19 ± 3)	Quartzites 20 ± 3	
	Slightly foliated		Migmatite (29 ± 3)	Amphibolites 26 ± 6		
	Foliated**		Gneiss 28 ± 5	Schists 12 ± 3	Phyllites (7 ± 3)	Slates 7 ± 4
IGNEOUS	Plutonic	Light	Granite 32 ± 3	Diorite 25 ± 5		
			Granodiorite (29 ± 3)			
	Dark	Gabbro 27 ± 3	Dolerite (16 ± 5)			
		Nonte 20 ± 5				
	Hypabyssal		Porphyries (20 ± 5)		Diabase (15 ± 5)	Peridotite (25 ± 5)
Volcanic	Lava		Rhyolite (25 ± 5) Andesite 25 ± 5	Dacite (25 ± 3) Basalt (25 ± 5)	Obsidian (19 ± 3)	
	Pyroclastic	Agglomerate (19 ± 3)	Breccia (19 ± 5)	Tuff (13 ± 5)		

* Conglomerates and breccias may present a wide range of m_i values depending on the nature of the cementing material and the degree of cementation, so they may range from values similar to sandstone to values used for fine grained sediments.

** These values are for intact rock specimens tested normal to bedding or foliation. The value of m_i will be significantly different if failure occurs along a weakness plane.

Table 2.8 Prediction of the σ_{ci} (Hoek, E.)

Grade*	Term	Uniaxial Comp. Strength (MPa)	Point Load Index (MPa)	Field estimate of strength	Examples
R6	Extremely Strong	> 250	>10	Specimen can only be chipped with a geological hammer	Fresh basalt, chert, diabase, gneiss, granite, quartzite
R5	Very strong	100 - 250	4 - 10	Specimen requires many blows of a geological hammer to fracture it	Amphibolite, sandstone, basalt, gabbro, gneiss, granodiorite, limestone, marble, rhyolite, tuff
R4	Strong	50 - 100	2 - 4	Specimen requires more than one blow of a geological hammer to fracture it	Limestone, marble, phyllite, sandstone, schist, shale
R3	Medium strong	25 - 50	1 - 2	Cannot be scraped or peeled with a pocket knife, specimen can be fractured with a single blow from a geological hammer	Claystone, coal, concrete, schist, shale, siltstone
R2	Weak	5 - 25	**	Can be peeled with a pocket knife with difficulty, shallow indentation made by firm blow with point of a geological hammer	Chalk, rocksalt, potash
R1	Very weak	1 - 5	**	Crumbles under firm blows with point of a geological hammer, can be peeled by a pocket knife	Highly weathered or altered rock
R0	Extremely weak	0.25 - 1	**	Indented by thumbnail	Stiff fault gouge

* Grade according to Brown (1981).

** Point load tests on rocks with a uniaxial compressive strength below 25 MPa are likely to yield highly ambiguous results.

2.4.2 Mohr Coulomb Failure Criterion

This criterion can be used to predict the effect of a given state of plane stress, when results of various types of tests are available for intact rock material. Coulomb (1776) assumed that the shear strength of rock and of soil are made up of two parts, a constant cohesion and a normal stress dependent frictional component. The shear strength that can be developed on a plane is expressed as follows.

$$\tau = c + \sigma_n \tan \phi$$

where

c = cohesion

σ_n = normal stress acting on the shear surface and

ϕ = frictional angle

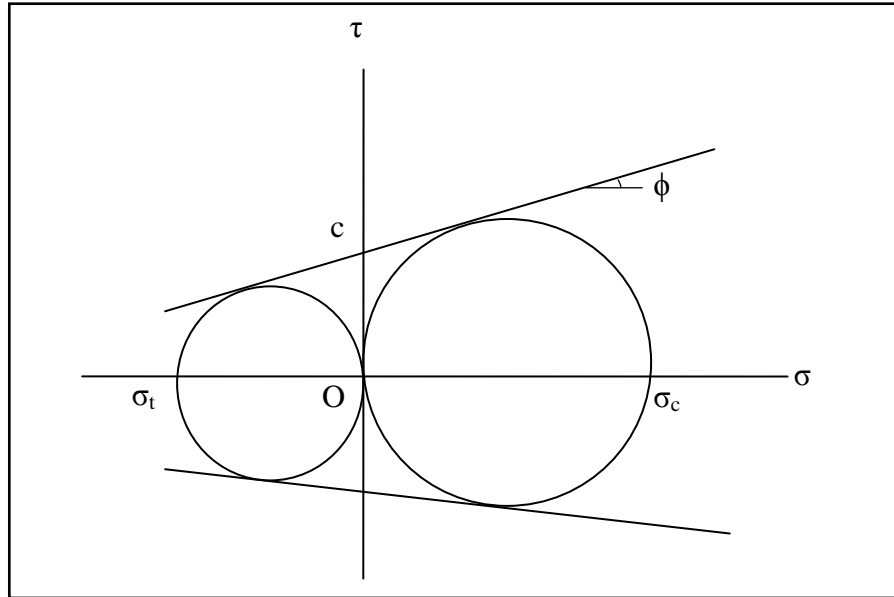


Figure 2.10 Mohr Coulomb failure criterion

If a tensile test and a compressive test have been conducted on a given material, the values of σ_t and σ_c of the ultimate strength in tension and in compression have been determined for that material. The state of stress corresponding to the rupture of the tensile test specimen can be represented in a Mohr-circle diagram by the circle intersecting the horizontal axis at O and σ_t (Figure 2.10). Similarly, the state of stress corresponding to the failure of the compressive test specimen can be represented by the circle intersecting the horizontal axis at O and σ_c . According to Mohr's criterion, a state of stress is safe if it is represented by a circle located entirely within the area bounded by the envelope of the circles corresponding to the available data.

According to Mohr' criterion the uniaxial compressive strength and uniaxial tensile strength are related to c and ϕ and defined by

$$\sigma_c = \frac{2c \cos\phi}{1 - \sin\phi} \quad (2.2)$$

$$\sigma_t = \frac{2c \cos\phi}{1+\sin\phi} \quad (2.3)$$

It should be noted that above equations are valid for intact rock specimens. Rock mass strength and deformation properties are different from intact rock strength and deformation properties because of discontinuities and geological conditions.

The uniaxial compressive strength, tensile strength, cohesion, frictional angle of rock mass of Gaziantep Seyrantepe caves are calculated by using the following relations suggested by Aydan et. al (2012).

The uniaxial compressive strength

$$\sigma_{cm} = \frac{\text{RMR}}{\text{RMR}+6(100-\text{RMR})} \sigma_c$$

The uniaxial tensile strength

$$\sigma_{tm} = \frac{\text{RMR}}{\text{RMR}+6(100-\text{RMR})} \sigma_t$$

Cohesion

$$c_m = \frac{\text{RMR}}{\text{RMR}+6(100-\text{RMR})} c$$

Frictional angle

$$\phi_m = \left(0.3 + 0.7 \frac{\text{RMR}}{100}\right) \phi$$

Mohr Coulomb failure criterion is used while doing the numerical analysis through software Plaxis in chapter 4. According to the relations suggested by Aydan et. al (2012) and to back analysis, the calculated rock mass properties are used in analytical calculations in chapter 6.

CHAPTER 3

SEYRANTEPE CAVES

3.1 Introduction

Gaziantep contains many man made caves having different sizes and shapes at shallow depths. Especially having the limestone of the geological formation of the city played an important role to occur these caves. This rock type is soft when cutting and can be easily shaped. It becomes harder when it is exposed to the air. These properties of the limestone make it the most popular construction material for many years until the arrival of concrete system. Since it is easy to reach the limestone in the region and a good material for constructions, stone quarries, commonly known as caves, were opened for supplying dimension stones to be used in the constructions in the half part of twentieth century in the city.

Seyrantepe caves are located in Seyrantepe neighbourhood of Gaziantep, next to the Abdulkadir Aksu Avenue (100th Street) separating Seyrantepe and Umut neighbourhoods. . Geographic map of Seyrantepe caves has been presented in Figure 3.1. The Latitude and Longitude of the caves are within $37^{\circ} 04' 25''$ N to $37^{\circ} 24' 56''$ E and $37^{\circ} 04' 19''$ N to $37^{\circ} 24' 58''$ E. The caves were excavated in a small hill, and were formed by manual caving into limestone as two floors. General view of Seyrantepe caves is shown in Figure 3.2

Seyrantepe caves consist of many caves. The top floor of Seyrantepe caves consist of eight large caves and seven small chambers. Figure 3.3 shows the location plan and the inner view of the eight large caves. Their spans are between 7 m and 38.5 m and average heights are 5.6 m. The shape of the caves is approximately rectangular. The roofs were declined following the bedding planes, so that the depth from the roofs to the ground surface varies from 2 m to 30 m. Each cave has some pillars to support its roof rock. The caves are connected to each other from inside. In short, Seyrantepe

caves have the following characteristics: shallow burried, soft surrounding rock, large span, approximately flat roof, little support and keeping a long term integrity.

Seyrantepe caves have used as animal shelters in the recent time. Then, these animal shelters are removed within the scope of landscape and the area is cleared. At the present Gaziantep Metropolitan Municipality consider using these caves as a Prehistory Museum. Although these caves excavated into the limestone have survived and kept their original integrity for years, observations on caves have also shown some indication of yielding and partial collapse at different scales at several location.



Figure 3.1 Location plan of the Seyrantepe caves



Figure 3.2 General view of Seyranteppe caves

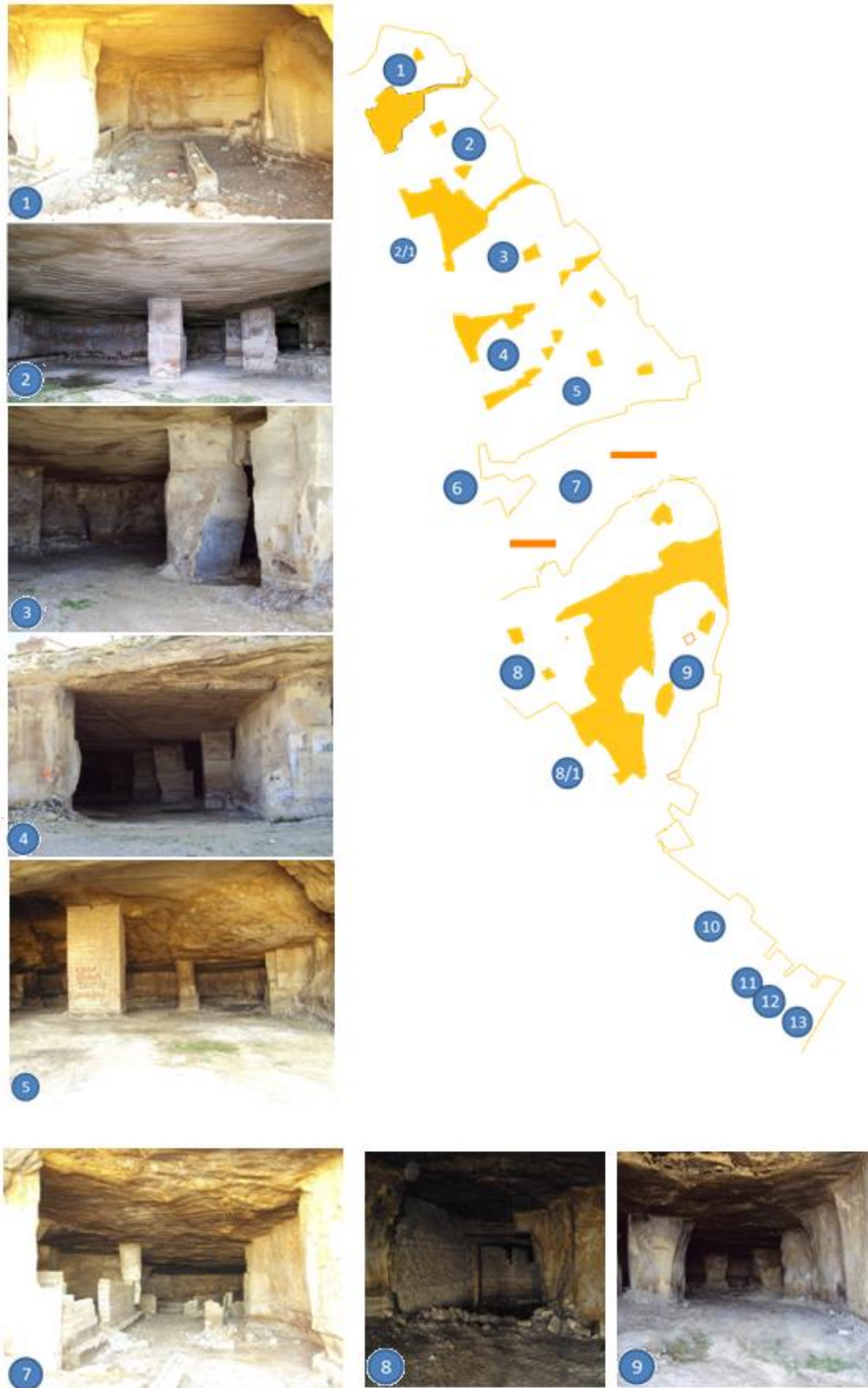


Figure 3.3 Location and inner view of the top floor of Seyrantep caves (photo: Gaziantep Metropolitan Municipality)

3.2 Geological Setting Of Seyrantepe Caves

MTA, Coşkun and Coşkun (2000), Terlemez et. al (1997) and Tolun and Pamir (1975) defined the general geology of Gaziantep. Geological map of Gaziantep province is given in Figure 3.4 by MTA. The geological formations of the city mainly involves Gaziantep and Yavuzeli formations. Yavuzeli formation consists of basalt deposits which have thickness varying between 0 and 150 m. Gaziantep formation consists of limestone which has thickness varying up to 300 m under the Yavuzeli formation. Limestone shows changing features and include some amount of marl and clay. Most of the caves in the city were carved into Gaziantep formation.

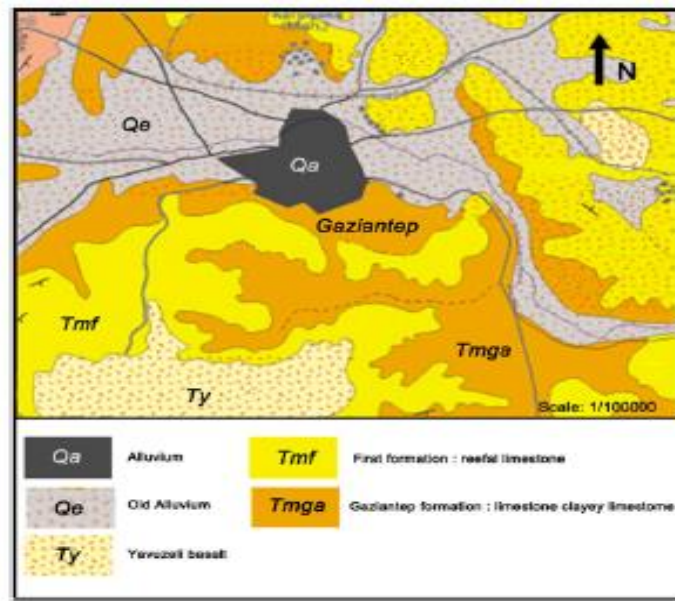


Figure 3.4 Geological map of Gaziantep, scale: 1/100,000 (MTA, 1997).

According to the visual geological investigation of the caves area, Seyrantepe caves are observed to carved into Oligocene and Mioocene age limestone. Seyrantepe caves are located within the Gaziantep formation which includes whitish to light gray and / or beige, soft strong, fresh to slightly weathered, thin to thick bedded, almost horizontal clayey, locally massive, marly limestone.

The joints are not closely spaced according to the ISRM and the persistence of the joints is rarely. Figure 3.5a and b shows the almost horizontal bedding plane of the limestone rock mass.

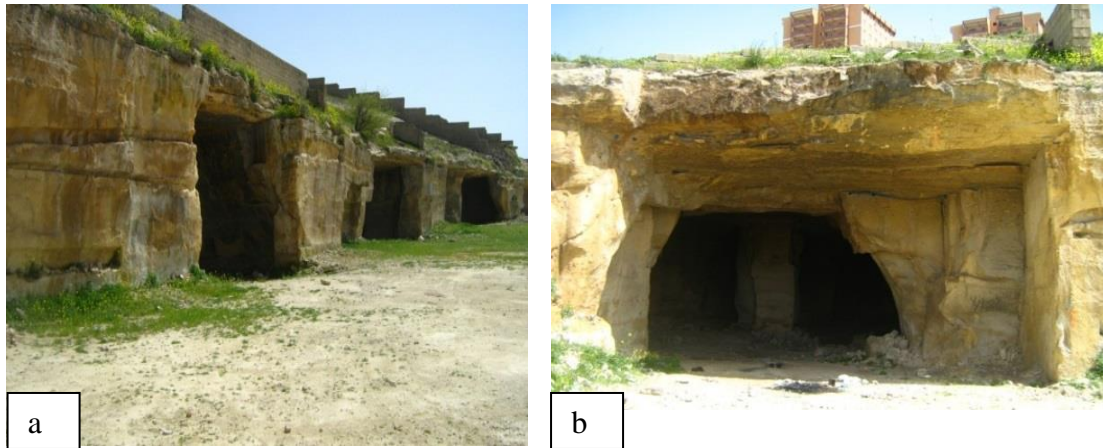


Figure 3.5. Horizontal bedding plane of Seyrantepe caves

3.3 Field Investigation

The field investigation consists of measurement geometric sizes of the caves and visual inspections of the rock mass around the caves. Measured geometric sizes of the caves were height, thickness of the roof and width. For this purpose 50 m capacity measuring tape and laser distance meter were used. Attention was given to details of the discontinuities such as, fill material in the cracks around the roof and wall, spacing and width of cracks.

The cracks was observed to develop mainly in the roofs, and rock pillars of the caves. The well-developed cracks in the cave roof are mainly near the cave entrance or around the pillars between caves (Figure 3.6a, Figure 3.6b, Figure 3.6c Figure 3.6d).

Rock mass around the caves consists of clayey marly limestone which is normally quite strong. But time factor and alteration occurring with atmospheric effects caused to reduce strength and the discoloration of the rock mass. Signs of this weakening are clearly observed entrance of the caves and supports. (Figure 3.6c)

In the recent time rock fall of the cave roof have occurred in cave no 5 as seen in Figure 3.7a.

Besides the cracks that have developed in the roofs, there are also some shear failures that have developed in the rock pillars between the caves. Figure 3.7b and Figure 3.7c show the shear failures of the rock pillars between cave 3 and 4, and cave 4 and 5 respectively .

Figure 3.8 a and Figure 3.8 b show the views of Cave No. 5 before and after the rock fall, respectively. It is clearly seen that there was a briquette wall before the rock fall. Its existence is also considered in the numerical analysis. Figure 3.9. also summarizes the location of the rock fall and shear failures of rock pillars along the section 1-1 of the caves.

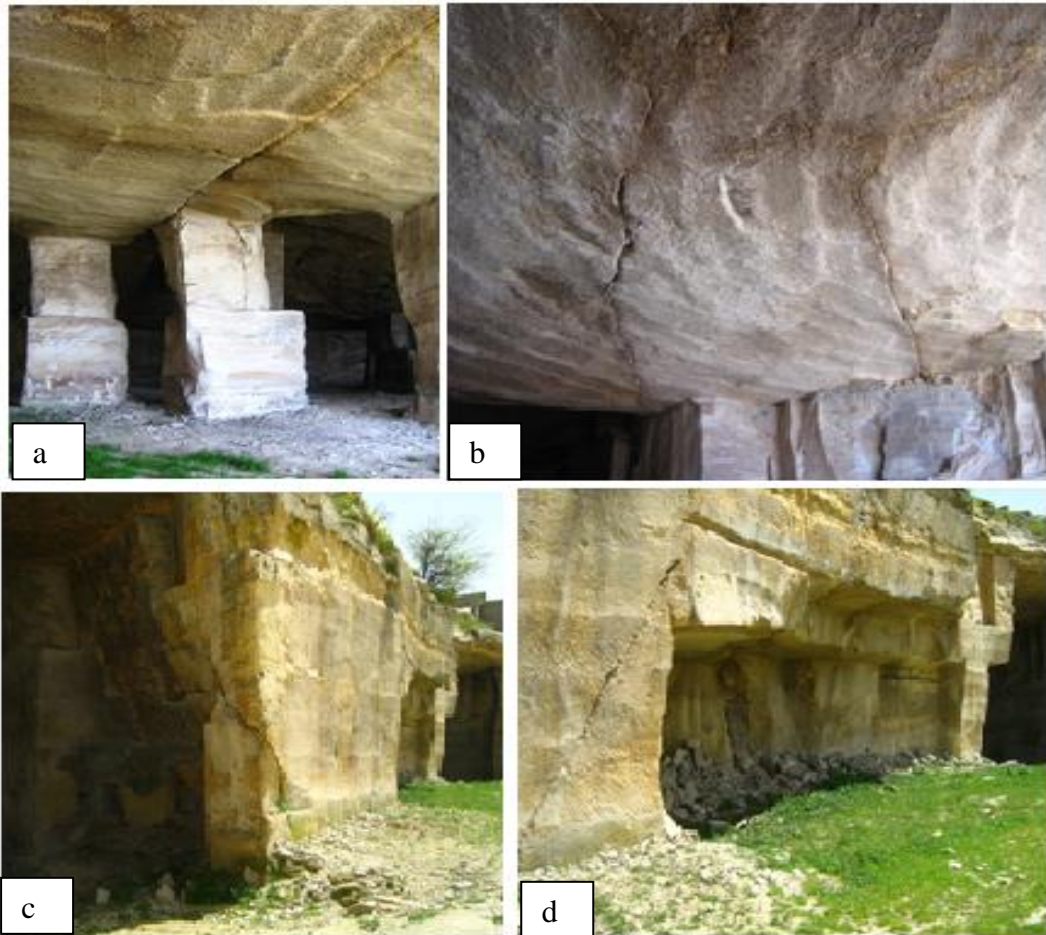


Figure 3.6 Cracks observed in the roofs and rock pillars of the caves and alteration.



Figure 3.7 Shear failures of rock pillars observed along the section 1-1 of the caves and rock fall in cave no 5

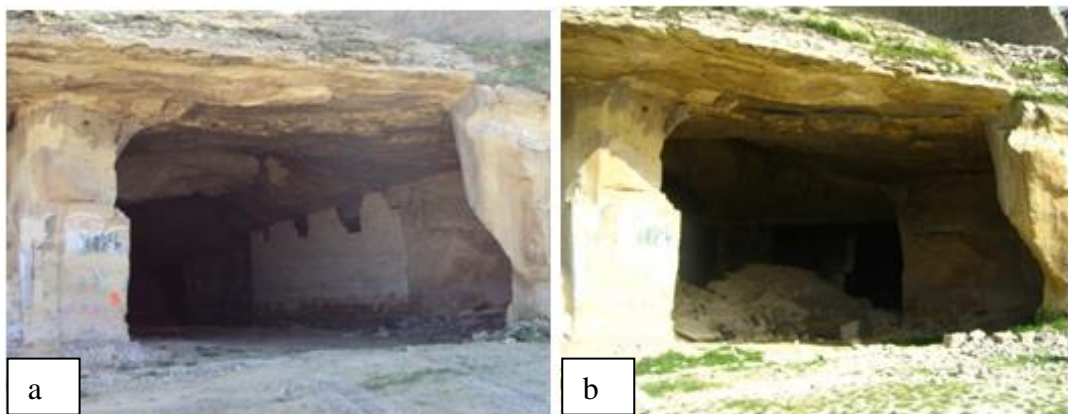


Figure 3.8. General view of the cave no 5 before and after the rock fall

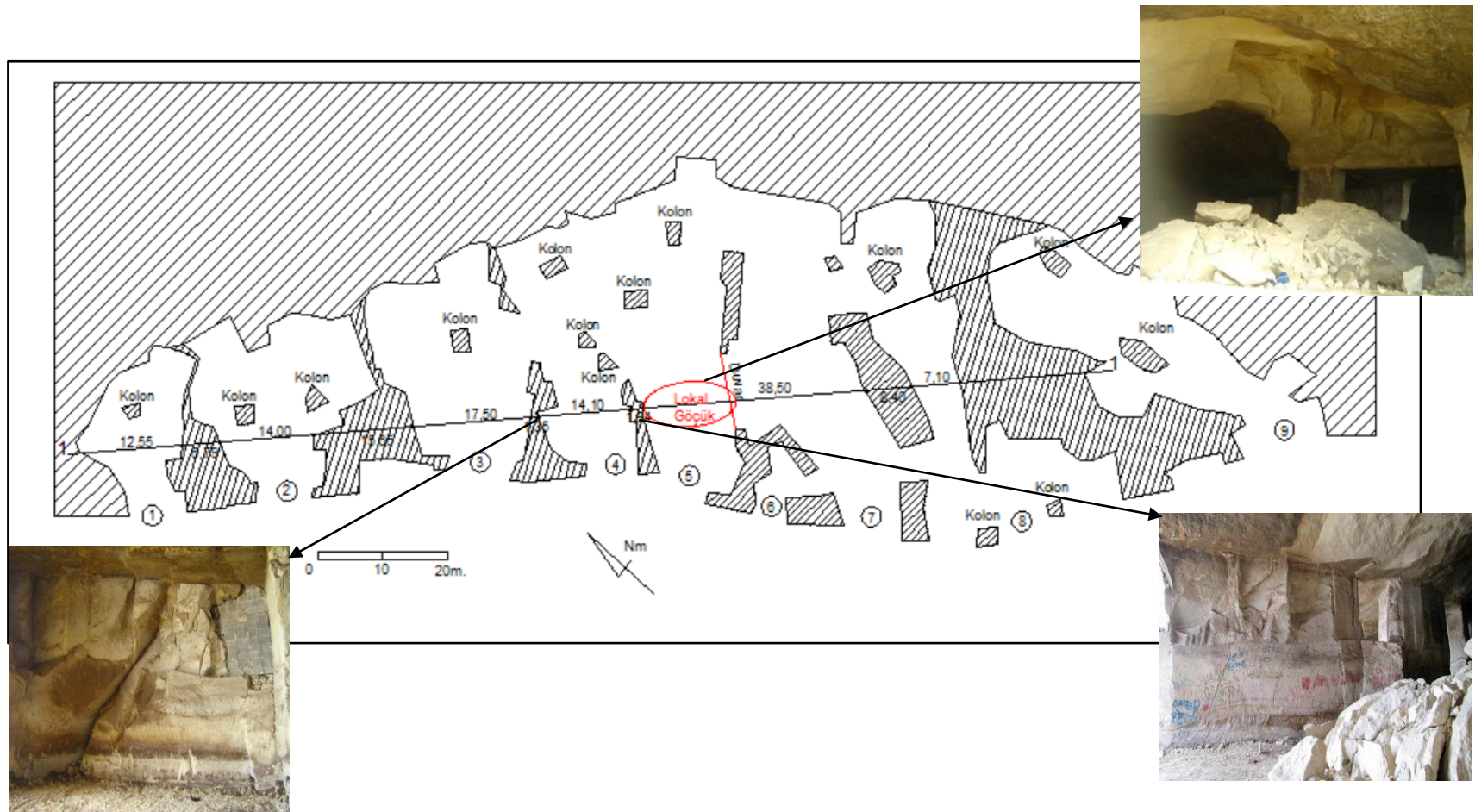


Figure 3.9. Location of the rock fall and shear failures of rock pillars along the section 1-1

3.4 Determination of the Rock Mass Geotechnical Parameters

3.4.1 Experimental Studies

To determine the necessary geotechnical parameters for rock mass, borings were performed by Gaziantep Metropolitan Municipality and rock mechanics tests were carried out on 20 good quality core samples obtained from the borings. Tests involved the determination of unit weight, uniaxial compressive strength (UCS), modulus of elasticity (E), poisson's ratio and water content of the surrounding limestone as intact rock under both dry and fully saturated conditions. These tests were carried out in accordance with the test procedures suggested by the International Society for Rock Mechanics (ISRM 1985). The results of the tests are presented in Table 3.1. Under dry condition, the average values of unit weight, uniaxial compressive, modulus of elasticity and poisson's ratio are 1.87 gr/cm³, 41.57 kg/cm², 9.85 GPa and 0.18, respectively. Under fully saturated condition, the average values of unit weight, water content (%), uniaxial compressive, modulus of elasticity and poisson's ratio are 2.19 gr/cm³, 18.35%, 26.92 kg/cm², 8.11 GPa and 0.13, respectively. It is clear from Table 3.1. that, under fully saturated condition, a decrease of greater than 60% occurs in strength compared with dry condition. In terms of strength and deformability, the intact rock is very weak according to ISRM (1985).

It is also important that the strength values given in Table 3.1. were obtained from intact core samples, but the rock mass strength of the limestone are expected to be lower than that of the intact rock due to the rock mass quality. This condition was taken into account by considering the Hoek-Brown failure criterion and rock mass classification systems. Then, calculated values are compared with back analysis results.

Table 3.1 Laboratory test results performed on the core samples obtained from borings

Borehole No	Sample depth (m)	Unit weight gr/cm ³	Water content (%)	UCS kg/cm ² (ISRM1 985)	Modulus of elasticity, E (GPa)	Poisson's ratio
SK-1 Saturated	2,00	2,18	18,69	27,9	8,0	0,12
SK-2 Saturated	3,00	2,21	18,01	28,5	8,2	0,13
SK-3 Saturated	2,00	2,17	18,16	27,2	8,4	0,14
SK-4 Saturated	3,00	2,19	18,60	26,5	8,1	0,13
SK-5 Saturated	2,00	2,20	19,12	26,6	7,9	0,14
SK-6 Saturated	3,00	2,20	19,60	25,9	8,3	0,12
SK-7 Saturated	2,00	2,21	17,23	26,5	8,4	0,12
SK-8 Saturated	3,00	2,18	17,30	26,1	8,0	0,13
SK-9 Saturated	2,00	2,17	18,36	26,5	7,9	0,14
SK-10 Saturated	3,00	2,19	18,45	27,5	7,9	0,11
SK-1 Dry	2,00	1,88	-	41,5	9,2	0,17
SK-2 Dry	3,00	1,87	-	42,5	10,3	0,19
SK-3 Dry	2,00	1,89	-	41,0	9,1	0,18
SK-4 Dry	3,00	1,85	-	40,0	9,8	0,17
SK-5 Dry	2,00	1,88	-	42,9	9,9	0,18
SK-6 Dry	3,00	1,87	-	43,2	10,1	0,19
SK-7 Dry	2,00	1,88	-	40,8	10,2	0,20
SK-8 Dry	3,00	1,89	-	41,1	10,5	0,19
SK-9 Dry	2,00	1,85	-	41,9	9,5	0,18
SK-10 Dry	3,00	1,86	-	40,8	9,9	0,19

3.4.2 Determination of the Rock Mass Geotechnical Parameters with Hoek-Brown Criterion

By using the relationship between the Hoek-Brown and Mohr-Coulomb criteria, the strength and deformation parameters of the Seyrantepe caves were obtained utilizing Hoek-Brown parameters.

The Hoek-Brown input parameters are σ_{ci} , m_i and the ranges of GSI values corresponding to the rock mass quality along with the rock mass disturbance factor, D.

Based on the rock mass description, the value of GSI is estimated from the contours given in Figure 2.9. The clayey, marly limestone rock mass surrounding Seyrantepé Caves is considered to possess the characteristics of a massive and very good rock mass for which an average GSI value of 85 is assigned. The uniaxial compressive strength of rock mass (σ_{ci}) is assigned as 4,08 MPa which is average value of UCS tests for dry samples. The Hoek- Brown constant m_i for the intact rock is determined from Table 2.7. as 10.

Table 3.2. presents the geotechnical properties of the very good quality clayey, marly limestone rock mass according to the Hoek-Brown failure criterion. The RocLab software with the tunnel application option was used to determine the rock mass geotechnical parameters since these parameters will be used to compare with the parameters obtained from the back analysis. The average tunnel depth of 70 m which is the elevation between the ground surface of the upper caves and top of the hill, an average rock unit weight of 18.34 kN/m^3 was used in RocLab. The average cohesion, internal friction angle, tensile strength, deformation modulus of the rock mass with $\text{GSI}=85$, $m_i=10$, $D=0$, and $\sigma_{ci}=4,08 \text{ MPa}$ is calculated as 366 kPa, 43.88° , 132 kPa and 9126.94 MPa, respectively. Information related to RocLab software is presented under the following title.

Table 3.2 Geotechnical properties of Seyrantepé caves rock mass as determine by the tunnel application option of RocLab.

Geotechnical Properties	Value
Intact rock strength (MPa)	4.08
Hoek-Brown constant m_i	10
Average GSI value	85
Disturbance factor, D	0
Hoek-Brown constant m_b	5.853
Hoek-Brown constant s	0.1889
Hoek-Brown constant a	0.5
$\sigma_{3\max}$ (MPa)	0.6173
Deformation Modulus (E_m ; GPa)	9126.94
Cohesion (c ; kPa)	366
Internal friction angle (ϕ ; °)	43.88
Rock mass tensile strength (kPa)	132

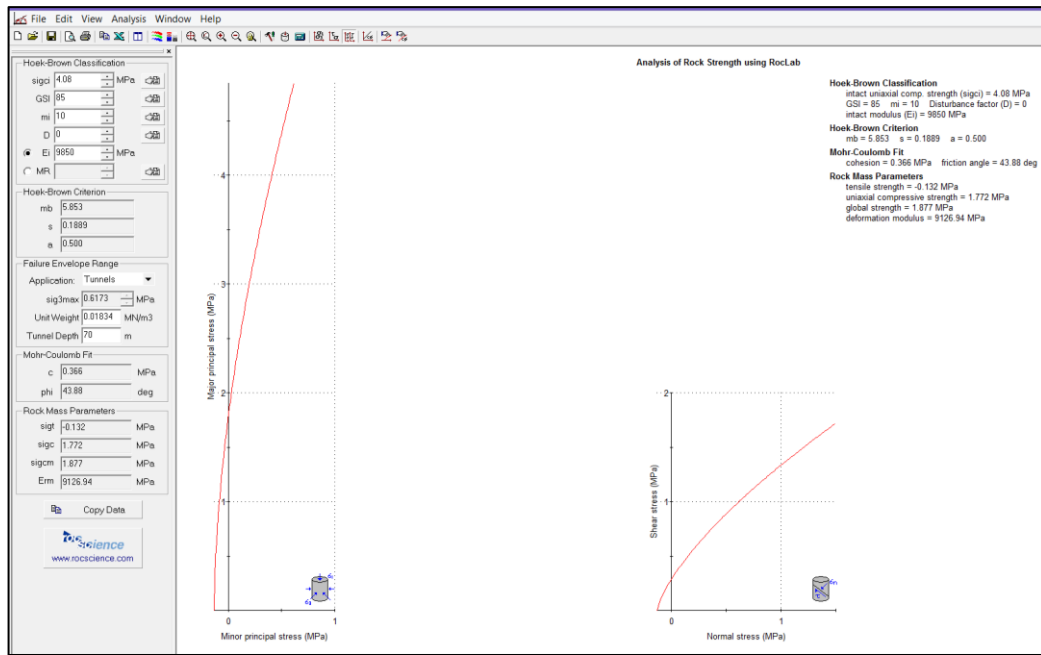


Figure 3.10 Main window of RocLab software used for input and output data

3.4.3 Determination of the Rock Mass Geotechnical Parameters with Mohr-Coulomb Criterion

The uniaxial compressive strength, tensile strength, cohesion and frictional angle of Seyrantepe caves rock mass were predicted from Mohr-Coulomb criterion using the relations suggested by Aydan et. al (2012) here. The results were presented below. RMR was assumed as 85.

The uniaxial compressive strength of Seyrantepe rock mass is

$$\sigma_{cm} = \frac{RMR}{RMR + 6(100 - RMR)} \sigma_c$$

$$\sigma_{cm} = \frac{85}{85 + 6(100 - 85)} 4.08 = 1.982 \text{ MPa}$$

The cohesion and frictional angle of Seyrantepe rock mass are calculated from the following equations by trial and error. The tensile strength is also computed from Equation 2.3 in terms of obtained shear strength pairs. Table 3.3 shows the geotechnical parameters calculated with trial and error.

$$\sigma_c = \frac{2c \cos \phi}{1 - \sin \phi}$$

$$1.982 = \frac{2c \cos\phi}{1 - \sin\phi}$$

As seen in Table 3.3 Mohr-Coulomb criterion gives greater values of cohesion and tensile strength than that of calculated from Hoek-Brown criteria for a constant frictional angle.

Table 3.3 Calculated rock mass geotechnical parameters with Mohr-Coulomb criteria

Uniaxial compressive strength of the rock mass (kPa)	Frictional angle ϕ	Cohesion, c, (kPa)	Tensile strength of the rock mass (kPa)
1982	35	516	537.2
1982	40	462	430.9
1982	43.88	422	359.3
1982	45	410.5	340.1

3.4.4 Back Analysis

Back analysis techniques as a practical engineering tool are nowadays often used in geotechnical engineering problems for determining the unknown geomechanical parameters, system geometry and boundary or initial conditions using field measurements of displacements, strains or stresses performed during excavation or construction works. Besides of these ways, back analysis can also be carried out by considering the failure modes (slide of the blocks in the sidewall, the collapse of the cave, falling of the cave roof, shear or tensile failure of the rock pillar etc.) of the underground spaces. In this case, plastic points in the numerical calculation output should give the failure shapes observed in the field.

In this study failure based back analysis was carried out on section 1-1 of Seyranteppe caves. Direct approach employed the trial values of the unknown parameters as input data, until the discrepancy between failure shape observed in the field and corresponding failure shape obtained from a numerical analysis is minimized. This procedure was continued until optimized values of all variables were determined. Optimum parameters were obtained by considering the failure shape observed in the

field. This approach is relatively simple and is suitable for determining of the rock mass geotechnical parameters. Then stability analysis using these optimized parameters was carried out.

Table 3.4 shows the results of rock mass properties of limestone according to back analysis output. Here, unit weight and poisson's ratio of rock mass were entered to the program by taking average values in Table 3.1 for dry core samples. Deformation modulus was taken from Table 3.2. according to Hoek-Brown failure criterion. For $c=420$ kPa, $\phi=40^\circ$, and $\sigma_t=185$ kPa quite compatible results with the real failure shape observed in the caves along the section were obtained from back analysis. In this thesis, rock mass geotechnical parameters obtained from back analysis results were used in further analysis.

Table 3.4 Geotechnical properties of rock mass based on back analysis

Material	Unit weight (kN/m ³)	Deformation modulus (GPa)	Poisson's ratio	Cohesion (kPa)	Internal friction angle (°)	Tensile strength (kPa)
Limestone	18,34	9126.94	0,18	420	40	185

CHAPTER 4

NUMERICAL ANALYSIS TO ASSESS THE STABILITY

4.1 Introduction

Rock mass in numerical modeling is separated into a large number of individual elements and are analyzed for rock stresses and deformation (Nilsen and Palmstrom, 2000).

Basic numerical modeling applied in rock mechanics problems are as follows

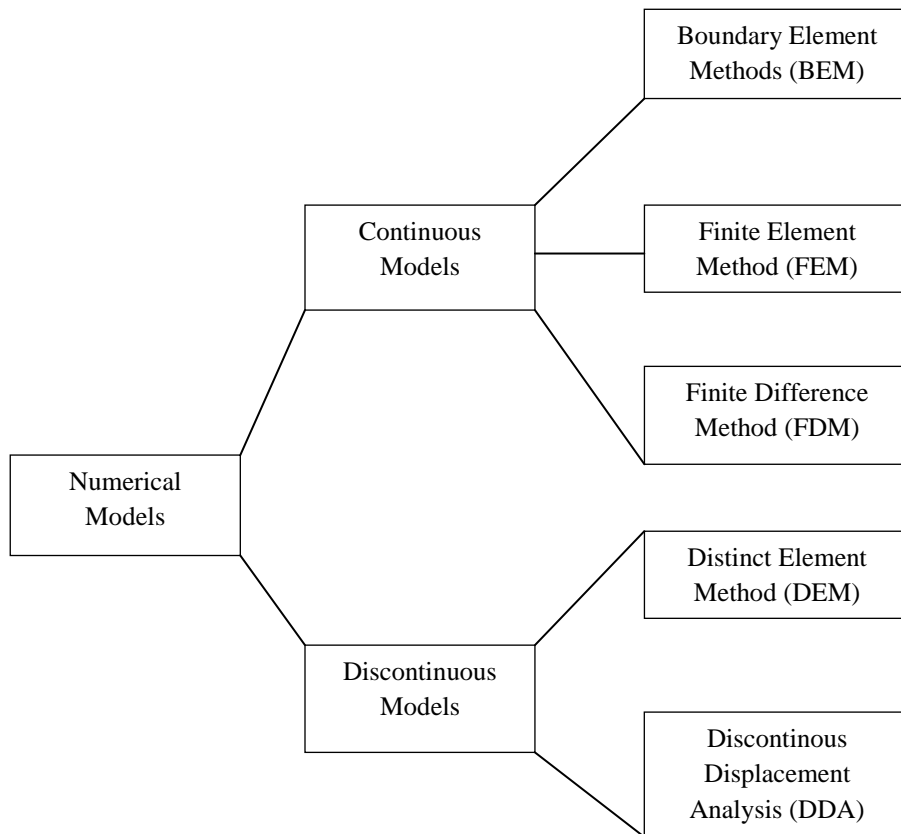


Figure 4.1. General Classification of Numerical Methods

Addition to above methods, some useful coupled modeling methods are as follows:

- FEM+BEM
- DEM+BEM
- DDA+FEM

4.2 Finite Element Method with Plaxis Software

The PLAXIS 2D is a Finite Element Code for soil and rock analyses that is capable of performing a practical analysis tool for use by geotechnical engineers considering linear and nonlinear structural analysis and anisotropic behavior of soils and/or rock. Plaxis is a finite element package that has been developed specifically for the analysis of deformation and stability in geotechnical engineering projects. The simple graphical input procedures enable a quick generation of complex finite element models, and the enhanced output facilities provide a detailed presentation of computational results. The calculation itself is fully automated and based on robust numerical procedures. This program is supporting two-dimensional analysis as well as axisymmetric analysis.

Also, there can be some numerical problems associated with using elasto-plastic materials in the models with extend values of material properties. These problems can be discovered when some of the computer runs failed to reach convergence. The user can assert these numerical problems by changing the type of iteration, method of integration, time curve, etc.

4.3 Modeling The Caves Using Plaxis Software

Figure 3.9. shows the location plan of the eight large caves of Seyrantepe for the upper story. Numerical analysis was carried out considering the worst section of the caves (i.e. widest span, minimum pillar thickness between adjacent caves and minimum rock cover above the caves) as indicated 1-1 section in Fig 3.9. Along the section the spans of the caves were measured in the field and also presented in Figure 4.2. The average height of the caves is approximately 5,6 m. The widest span was measured as 38,5 m after collapsing the briquette wall. The roofs were declined following the bedding planes, so that the depth from the roofs to ground surface was determined as 9 m.

Plaxis 8.2 was used for modeling the caves. The sizes of the caves and material properties of the caves were considered as input data of the software. Mohr-Coulomb failure criterion was selected from those available in Plaxis to describe the failure behavior of rock. Limiting states of stress are described by means of σ and c . Deformation modulus of the rock mass was used rather than intact rock deformation modulus due to discontinuities of rock. The initial stress were generated from at rest earth pressure coefficient $K_0=(1-\sin\phi)$ where ϕ is the friction angle in terms of effective stress. Since ground water table is well below the base of the caves the effect of pore water pressure was not included in the analysis.

Plaxis incorporates a fully automatic mesh generation procedure, in which the geometry is divided into elements of the basic element type. During the generation of the mesh, 15- node triangular elements were selected in preference to the alternative of 6 noded versions in order to provide greater accuracy in the determination of stress. Five different mesh densities are available in the program ranging from very coarse to very fine. Analyses were made using fine mesh density. Model is set to plane strain.

Boundary conditions play an important role in Plaxis. In principle, all boundaries must have one boundary condition in each direction. That is to say, when no explicit boundary condition is given to a certain boundary, the natural condition applies, which is a prescribed force equal to zero and a free displacement. To avoid the situation where the displacements of the geometry are undetermined, some points of the geometry must have prescribed displacements. The simplest form of a prescribed displacement is a fixity (zero displacement), but non-zero prescribed displacements may also be given. In this work, for boundary condition, standard fixities button was used on the toolbar of Plaxis. Standard fixities allow a horizontal fixity in vertical geometry lines, and a full fixity in horizontal geometry lines. The finite element mesh and boundary conditions along section 1-1 are shown in Figure 4.3. Global factor of safety of the caves against failure was calculated using Phi-c reduction option available in Plaxis. In the Phi-c reduction approach, the strength parameters $\tan\phi$ and c of the soil are successively reduced until failure of the structure occurs. The total multiplier ΣM_{sf} is used to define the value of the soil strength parameters at a given stage in the analysis.

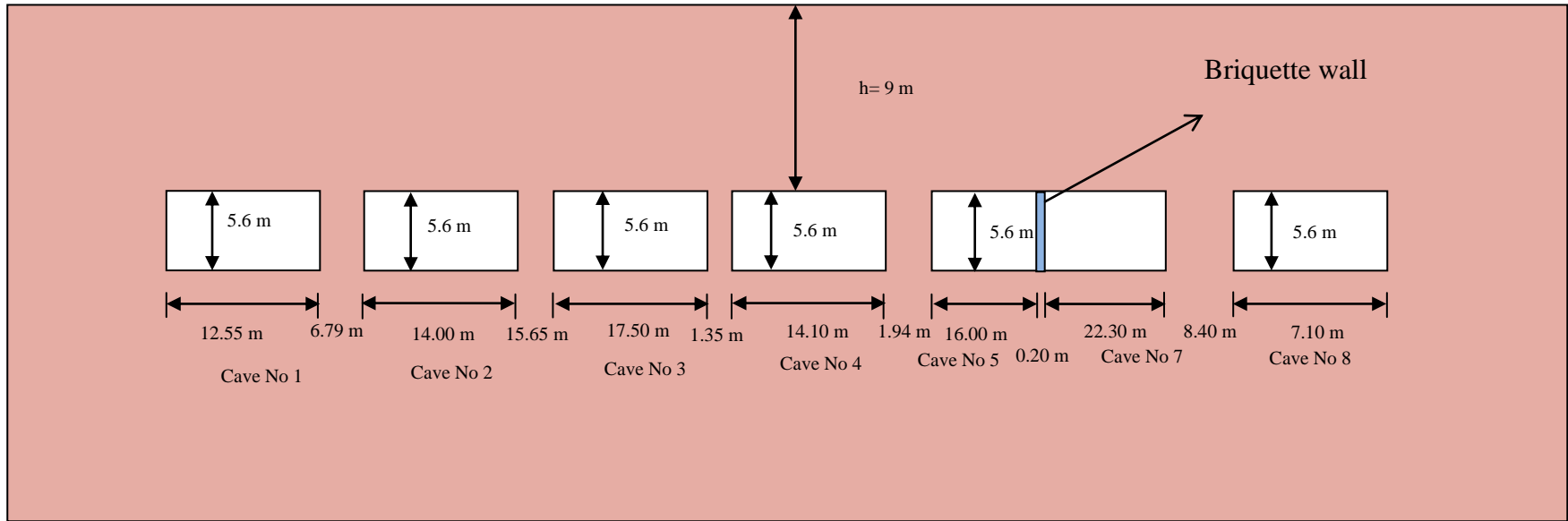


Figure 4.2 Dimesion of the caves along section 1-1

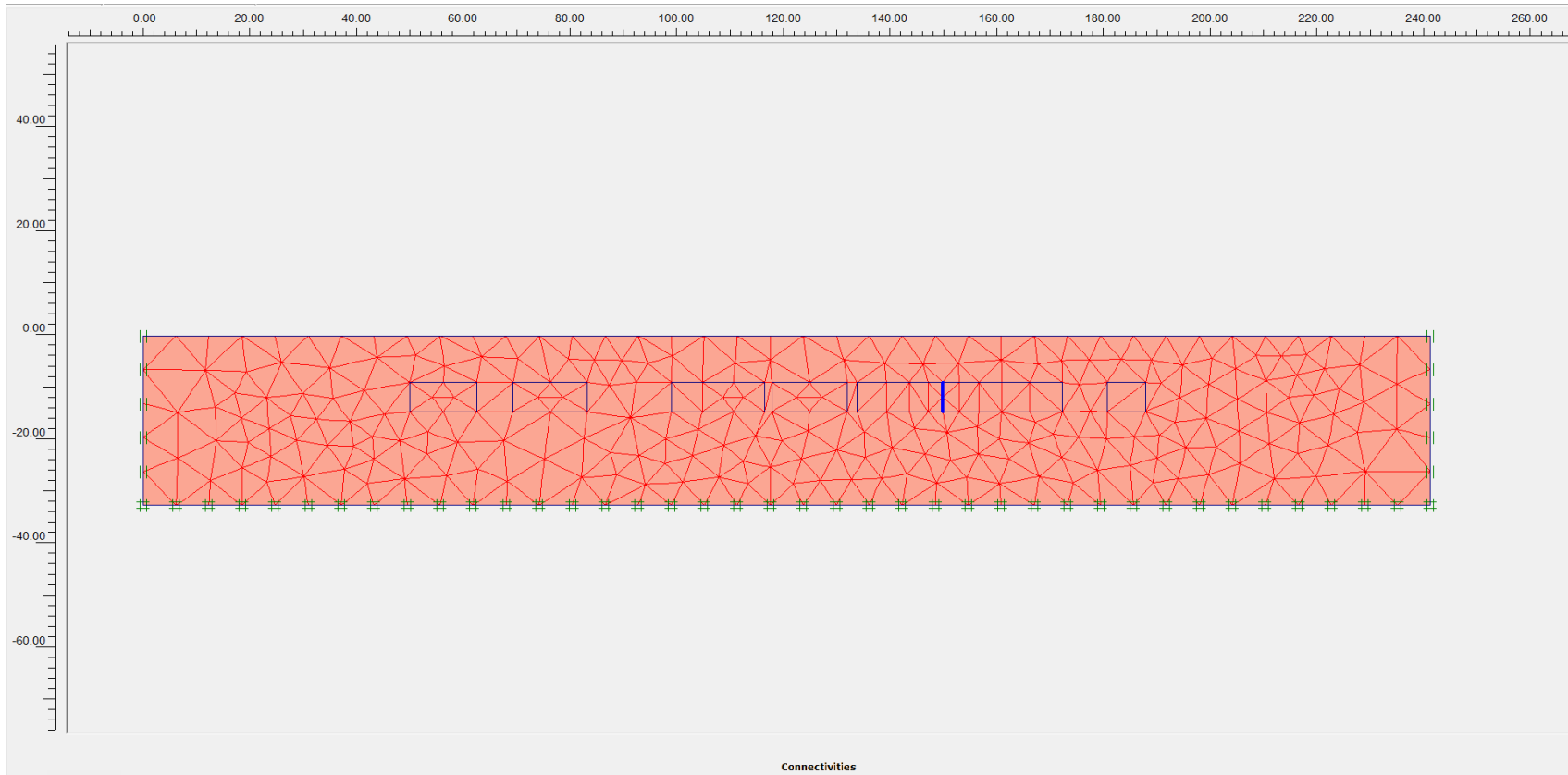


Figure 4.3 Finite element mesh and boundary conditions along section 1-1

$$\Sigma M_{sf} = \frac{\tan\theta_{input}}{\tan\theta_{reduced}} = \frac{c_{input}}{c_{reduced}}$$

Where the strength parameters with the subscript ‘input’ refer to the properties entered in the material sets and parameters with the subscript ‘reduced’ refer to the reduced values used in the analysis. ΣM_{sf} is set to 1.0 at the start of a calculation to set all material strengths to their unreduced values.

A phi-c reduction calculation is performed using the load advancement number of steps procedure. The incremental multiplier M_{sf} is used to specify the increment of the strength reduction of the first calculation step. This increment is by default set to 0.1, which is generally found to be a good starting value. The strength parameters are successively reduced automatically until all additional steps have been performed. It must always be checked whether the final step has resulted in fully developed failure mechanism. If that is the case, the factor of safety is given by

$$FS = \frac{\text{available strength}}{\text{strength at the failure}} = \text{value of } \Sigma M_{sf} \text{ at failure}$$

The geotechnical parameters given in Table 3.4 were used in numerical analysis due to obtaining quite compatible results with the real failure shape observed in the caves along the section. The wall was modeled as a plate element in Plaxis. Elastic behaviour was selected in Plaxis. The mechanical properties of briquette wall were assumed as given in Table 4.1. Empirical approach of Koksall vd, (2004) was used to determine the modulus of elasticity of the wall. According to the this approach, modulus of elasticity, poisson’s ratio were assumed as 2500 MPa and 0,30, respectively. Wall thickness was taken as 0.2 m. The other mechanical properties of wall were calculated as following.

Assumption of the wall element:

E: 2500 MPa

Wall thickness (t): 0,20 m

Dead weight of wall (w): 7 kN/m/m

Area for 1 m length (A): $0,20 \times 1 = 0,20 \text{ m}^2$

The calculations:

$$\text{Moment of Inertia (I)} = \frac{bt^3}{12} = \frac{1 \times 0.20^3}{12} = 6.67 \times 10^{-4} \text{ m}^4$$

$$EA = 2500 \times 10^3 \times 0.20 = 5 \times 10^5 \text{ kN/m}$$

$$EI = 2500 \times 10^3 \times 6.67 \times 10^{-4} = 1666.67 \text{ kNm}^2/\text{m}$$

Table 4.1 Mechanical properties of briquette wall

Material	Modulus of Elasticity (MPa)	Wall thickness, d, (m)	EA (kN/m)	EI(kNm ² /m)	w (kN/m/m)	v (poisson's ratio)
Briquette wall	2500	0,2	5x10 ⁵	1666,67	7	0,3

After determining these parameters, back stability analysis was performed. Input parameters obtained from back analysis were used in back stability analysis of section 1-1 of the cave. For the initial stress, K_0 was calculated as 0,357 from at rest earth pressure coefficient $K_0 = (1 - \sin \theta)$ where θ is 40°.

4.4 Results of Analysis

Output results obtained from the analysis of section 1-1 is shown in Figure 4.4 to Figure 4.12. Figure 4.4 shows the plastic points obtained from the analysis of section 1-1. Here, in interpretation module of software, elements which fails in shear is indicated by red whereas yielded elements in tension is indicated by white with Mohr Coulomb failure criterion. As seen in Figure 4.4 cave roof between pillar (between cave 4 and cave5) and briquette wall fails in tension. Rock pillars between cave 3 and 4, and cave 4 and 5 fail in shear.

Figure 4.5 shows the relative shear stresses shadings. As seen here, extreme relative shear stressess concentrate at the pillars between cave no 3 and cave no 4, and cave no 4 and cave no 5. Concentrated shear stresses are also shown around the right corner of the cave no 7. When the extreme relative shear stress has reached to 1,00 at any point, it gives a shear failure line. The relative shear stress points confirm the plastic point locations as seen in Figure 4.4.

As it can be seen in Figure 4.6, extreme total displacement is found as 13.42 mm. Vertical displacements occur at the cave roof, above the wall, towards the inside of the cave and the maximum horizontal displacements occur at the ground surface, above the cave no 7 towards the cave no 1. The maximum vertical displacement is 3,46 times higher than the maximum horizontal displacement.

Maximum and minimum principal stresses are presented in Figure 4.9. Value of these principle stresses determines how the rock mass behaves with induced stresses. Comparative study of those principle stresses having different opening geometry may somehow help to predict the relative stability condition. Fig 4.9 illustrates a natural rock arch located approximately ground level above the flat roof surface. A real loosened zone is formed below the natural rock arch, which can not transmit any load to the supports.

Maximum axial force, shear force and bending moment in the wall are presented in Figure 4.10 through Figure 4.12. As it is seen, maximum axial force in the wall is found as $-1,24 \times 10^3$ kN/m. Maximum shear force and bending moment are also found as $4,28 \times 10^{-9}$ kN/m and $5,63 \times 10^{-9}$ kN/m/m, respectively. The factor of safety against failure of this section was calculated as 1,45 using phi-c reduction option in Plaxis.

In this work, it is also investigated the effects of the adjacent caves on failure and the stability. For this purpose, single isolated opening of cave no 7 has been discussed. Figure 4.13 shows the failure zone around the cave no 7 without considering the adjacent cave. In this case tension cut off points occur at the midspan of the cave. Factor of safety against failure in this case is calculated as 1,86. When considering the effects of the adjacent caves, plastic points around the caves is found as seen in Figure 4.14. Here tension cut off points occur at the roof between the pillar and wall. Moreover pillars between cave no 3 and 4, and 4 and 5 fail in shear. Factor of safety against failure in this case is calculated as 1,45 as mentioned before.

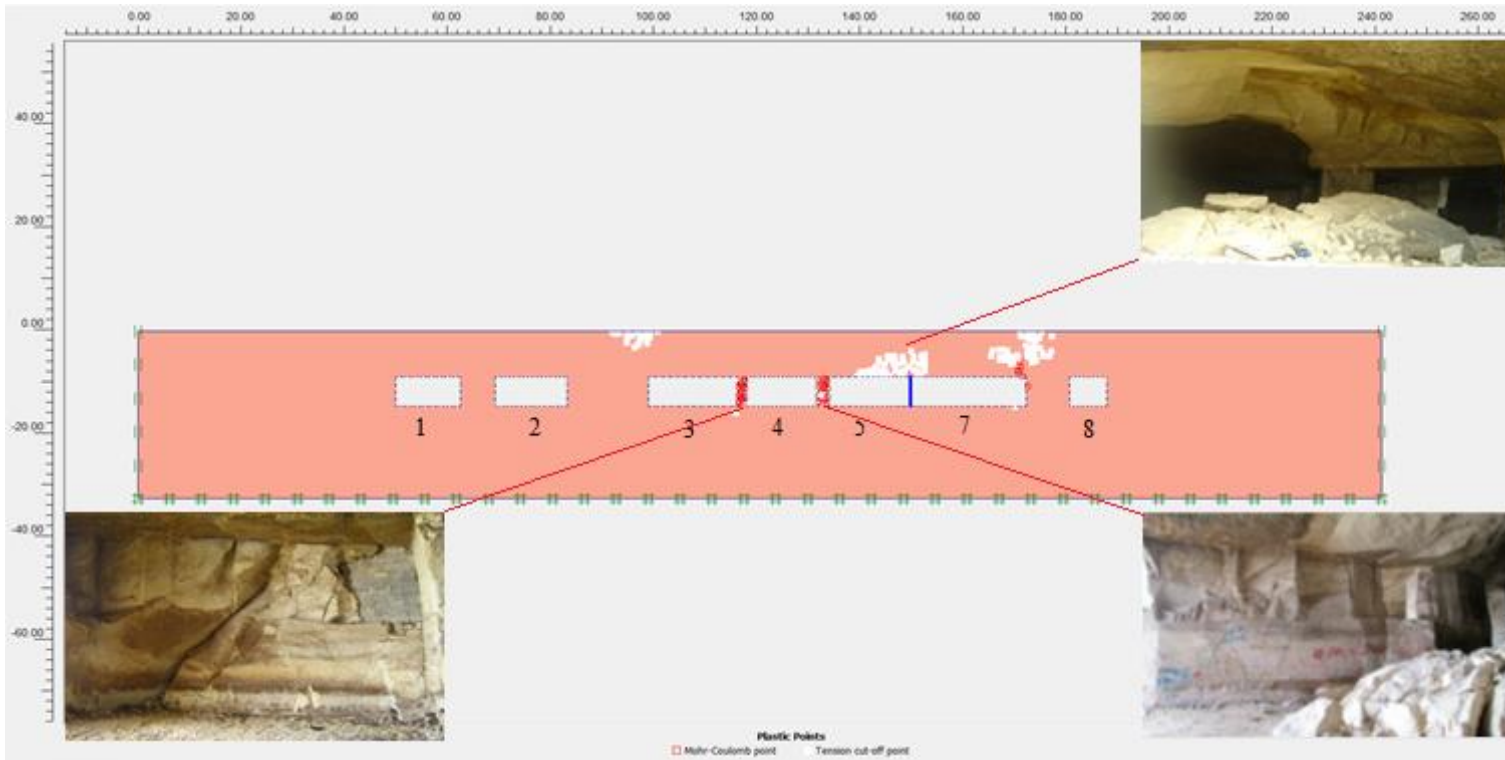


Figure 4.4 Plastic points based on FEM analysis and failure zones observed in situ

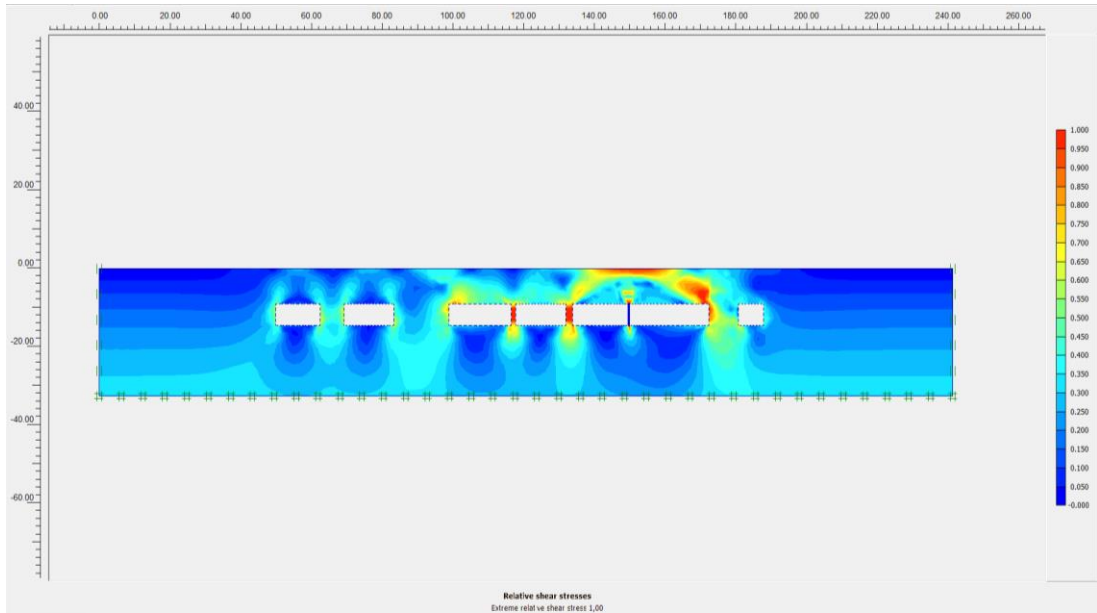


Figure 4.5 Relative shear stresses

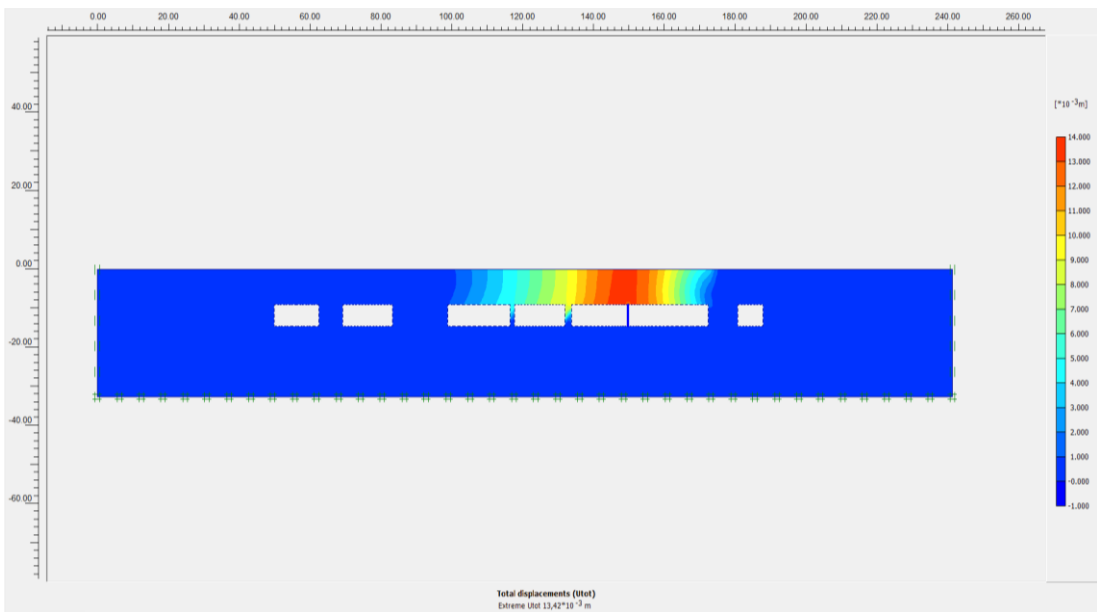


Figure 4.6 Total displacements

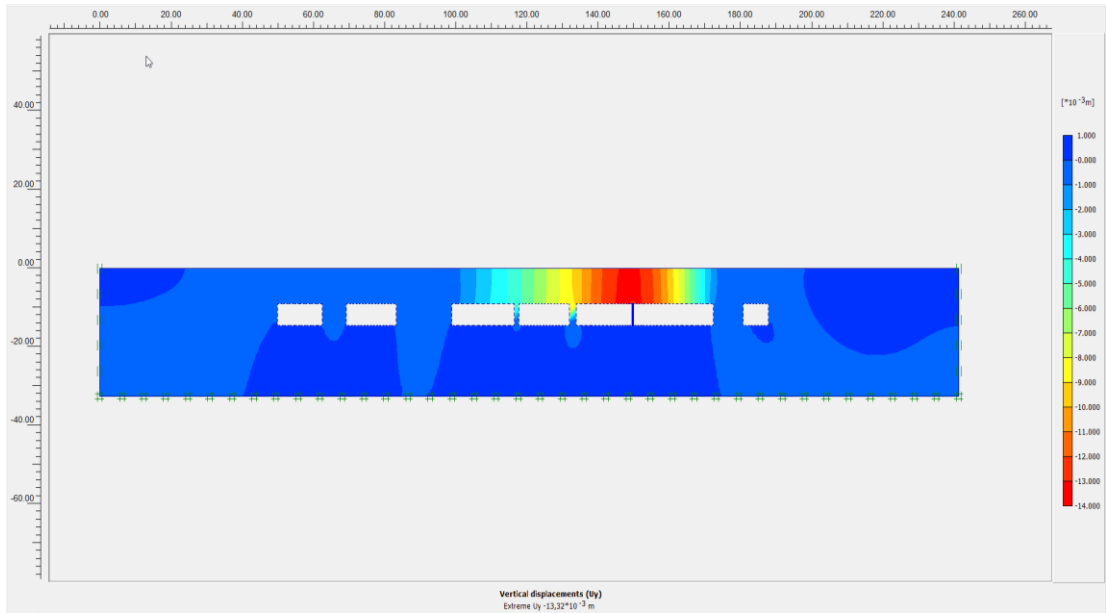


Figure 4.7 Vertical displacements

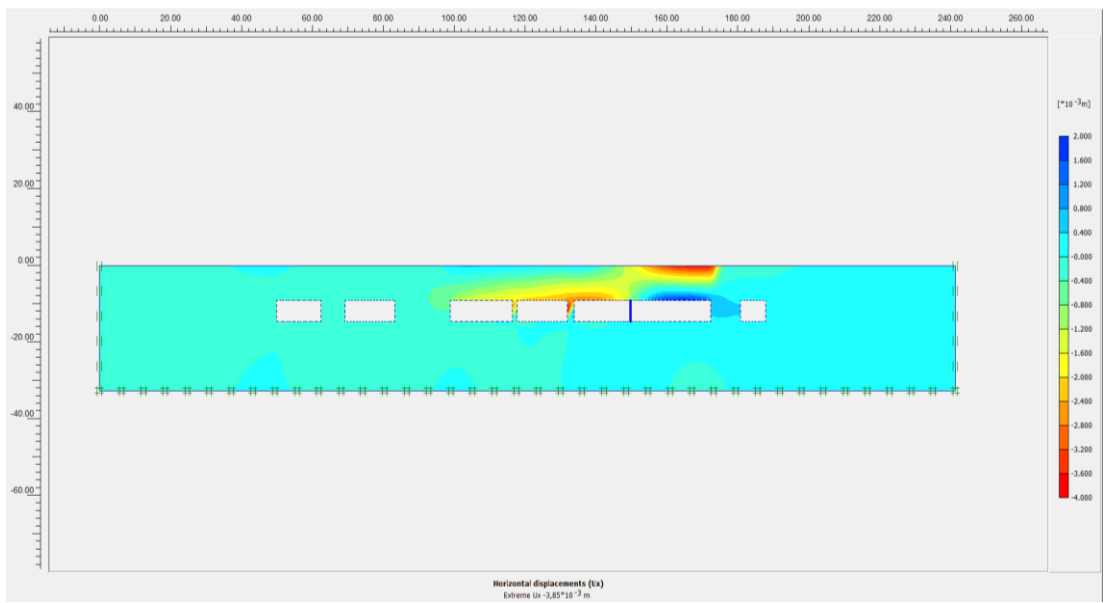


Figure 4.8 Horizontal displacements

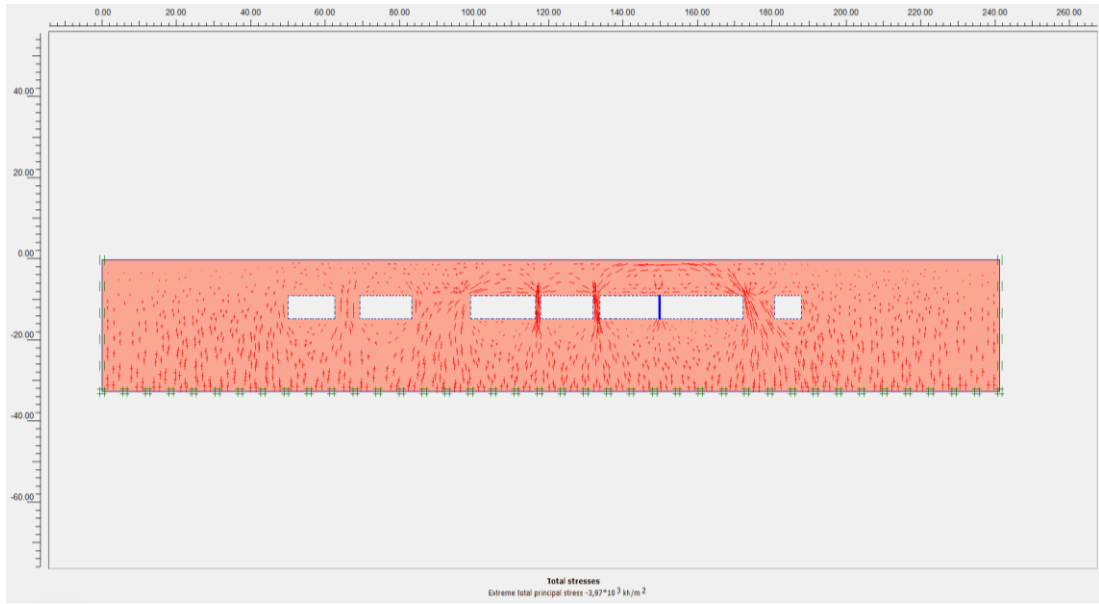


Figure 4.9 Principal stresses

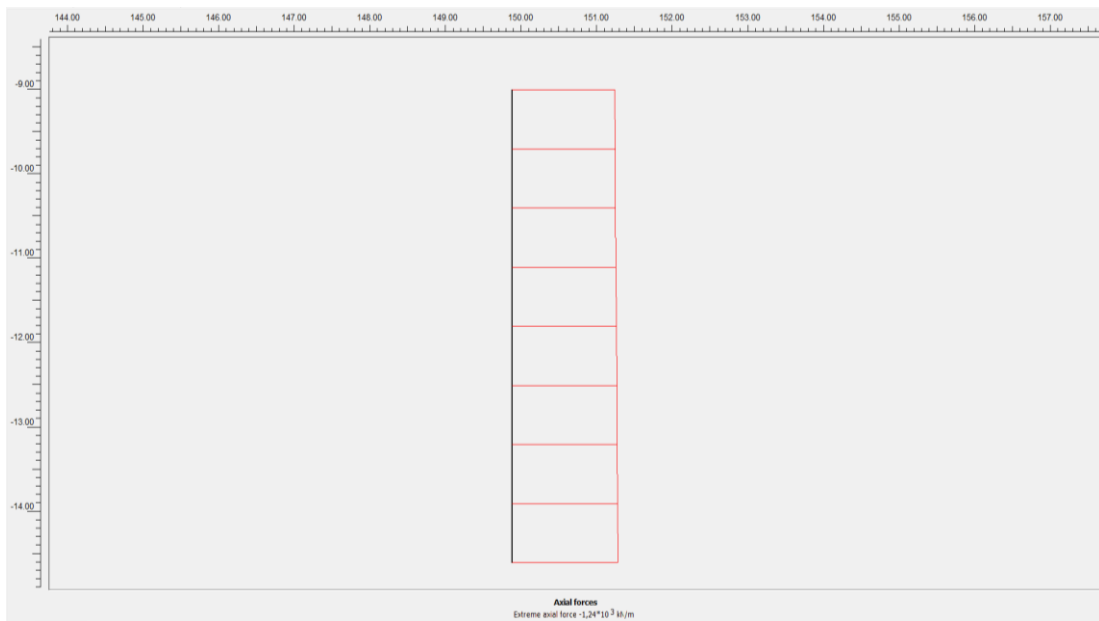


Figure 4.10 Axial forces in the wall

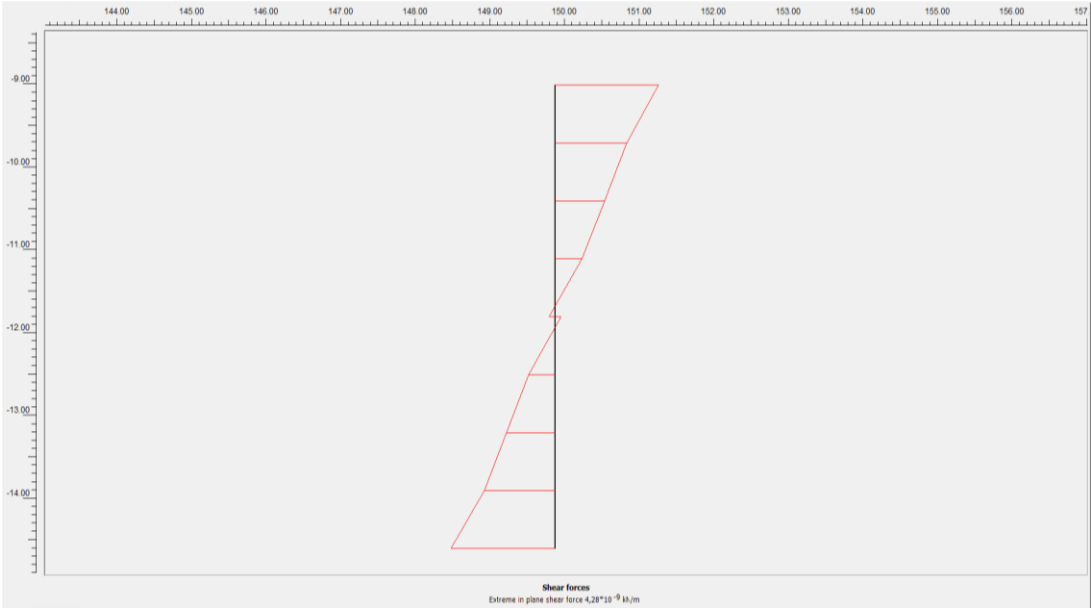


Figure 4.11 Shear forces in the wall

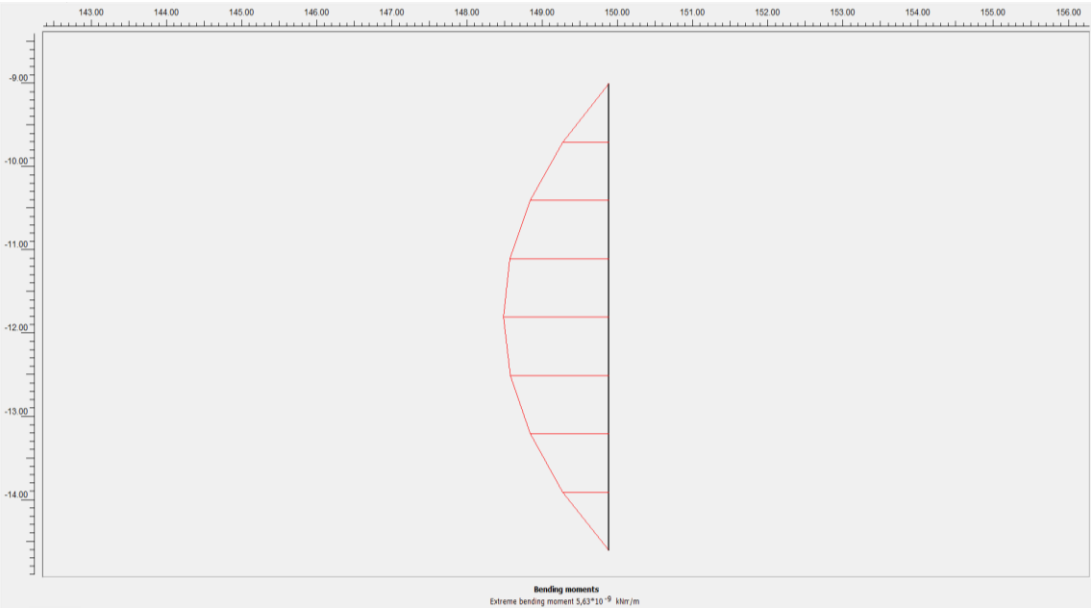


Figure 4.12 Bending moments in the wall

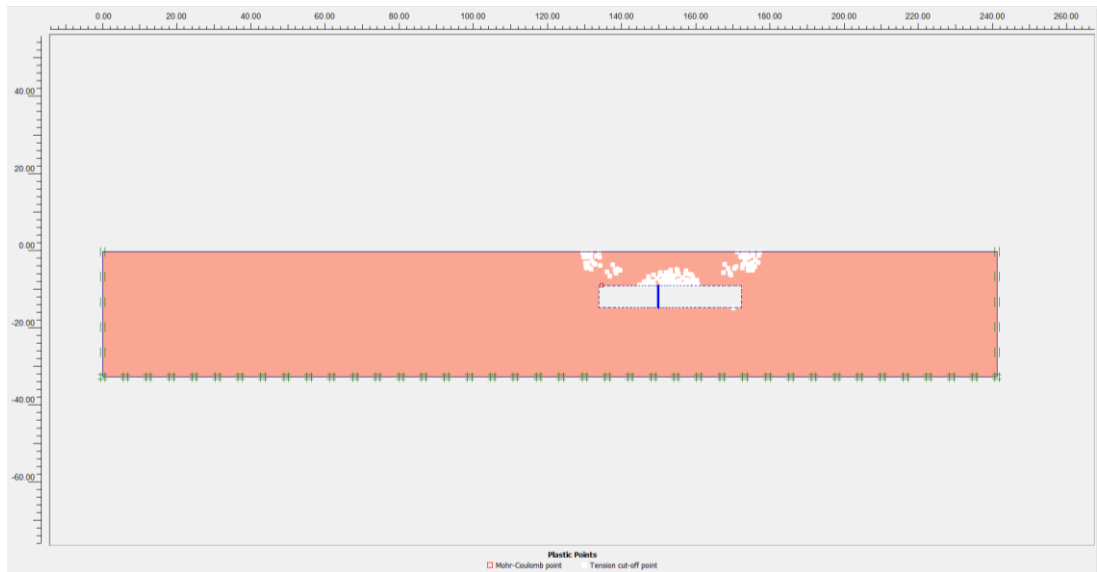


Figure 4.13 The failure zones around the cave no 7 without considering the adjacent caves

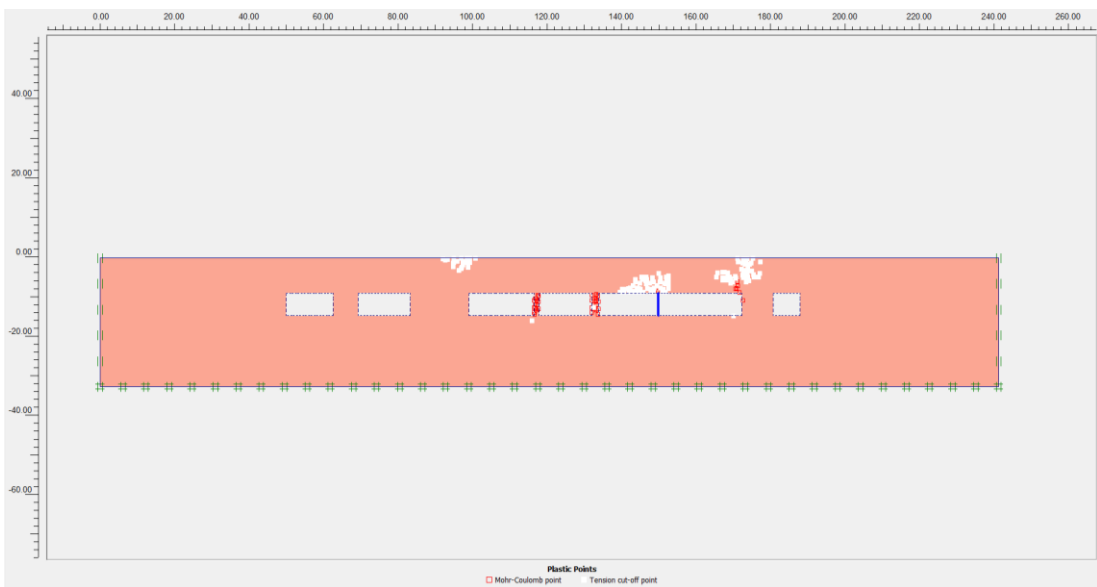


Figure 4.14. The failure zones around the cave no 7 with considering the adjacent caves

CHAPTER 5

EMPIRICAL APPROACHES TO ASSESS THE STABILITY

In this chapter various empirical stability assessments containing rock mass classification system are carried out.

5.1 Assessment of the Stability with Rock Mass Classification Systems

Empirical stability assessments in this section are the assessments which are made using the Rock Mass Rating (RMR) system, Rock Tunneling Quality Index (Q).

By using RMR system, the stand up time of any underground span can be determined. Following Figure 5.1 shows the relationship between the stand up time, RMR value, roof span, and required support system for the section 1-1 of Seyrantepe caves.

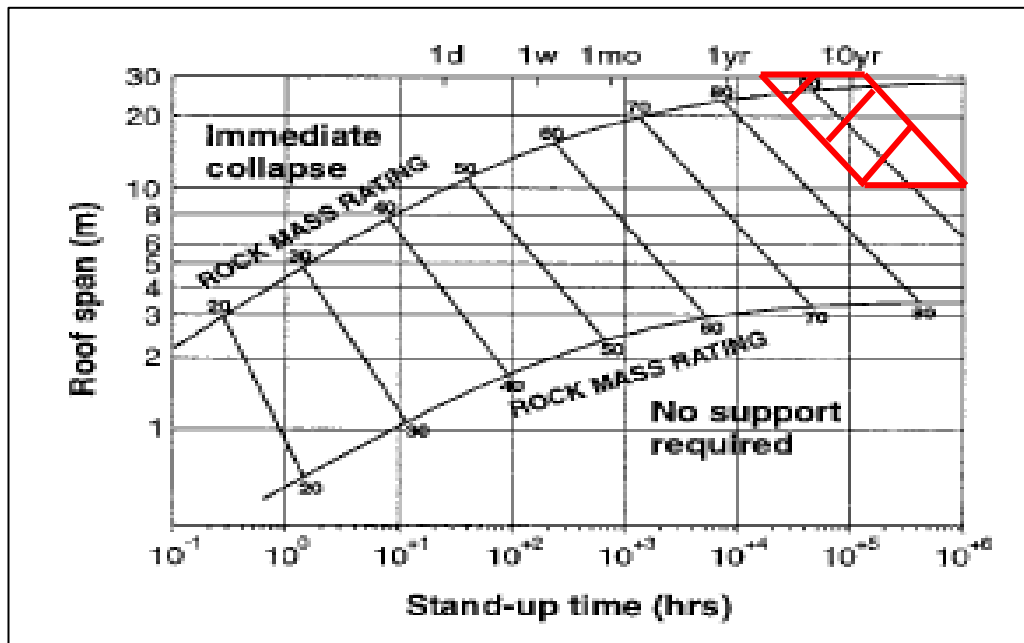


Figure 5.1 The relationship between roof span and stand up time for different RMR value of Seyrantepe caves

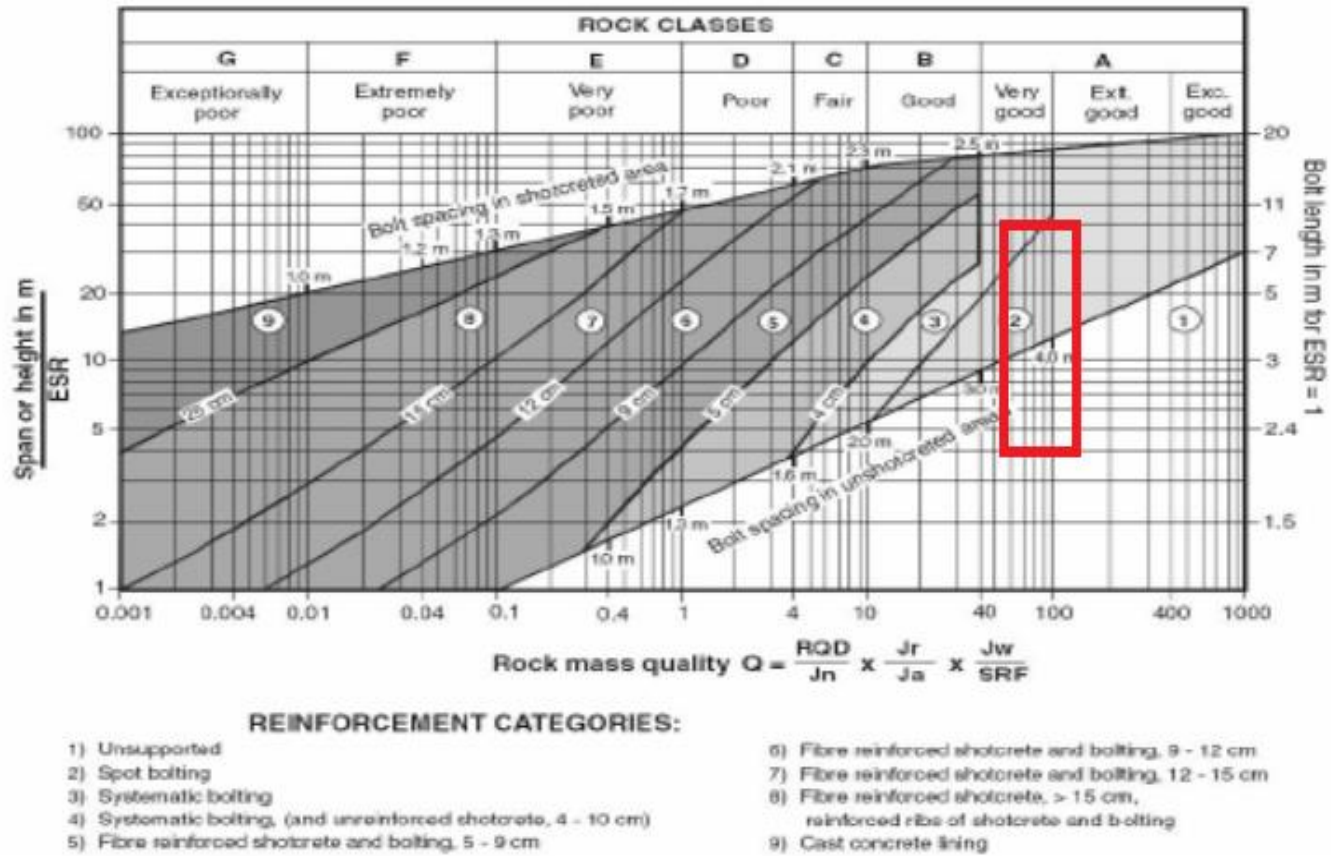


Figure 5.2 Estimated support categories based on the tunnelling quality index Q

According to the Figure 5.1, unsupported stand up time for the Seyrantepe caves is approximately 4 or 5 years. But the caves have stood up without any support for many years. and except local failure, they still keep their stability. As seen in Figure 5.1 an immediate collapse is also expected for roof spans more than 10 m. According to these differences, unsupported stand up phenomenon suggested by Bieniawski (1989) contains rock fall even though not effect the stability. This approach is quite conservative to determine the unsupported stability time in fact. Aydan (2012) stated that using the RMR, Q, RSI, rock mass classification systems are not suitable for natural cave type underground spaces to determine unsupported stability time because of the same problems. Figure 5.2 also shows the rock support chart of Seyrantepe caves according to the Q system.

Calculated supports system are:

- 1) Unsupported
- 2) Spot bolting
- 3) Systematic bolting

Generally, rock mass classification system suggests to use the rock supports for many openings of the caves. But it can be said that validity of the using rock support is quite controversial. Empirical approaches commonly help to determine the rock support system and generally use to this purpose. But the stability differs from determination of the rock support in one way. Stability of opening largely depends on the geometry of the opening and rock mass strength. With the stability approach, a factor of safety and risk factor level against failure are determined.

In scientific publications there are various empirical approaches between RMR, Q, and allowed span or height.

Barton et al. (1974) expressed the relationship between unsupported span and Q as follows.

$$L=2.Q^{0.4}$$

Barton (1976b) suggested the following equation based on his observation on Carlsbad karst caves in America, concerning the relationship between unsupported span and Q value.

$$L=66\log Q + 2$$

Tokashiki (2011) and Aydan and Tokashiki (2011) proposed some empirical relations between RMR and limit span for different stability categories, which are directly applicable to caves in Ryukyu Islands. The categories of stability modes are illustrated in Table 5.1. The boundary of each categories gives the following two equations to determine the limit span as a function of RMR. The formulas are given as linear and power functions.

The formula of linear function:

$$L = a.RMR + b$$

The formula of power function:

$$L = a.RMR^b$$

a and b are the empirical coefficients. Table 5.2 presents the values of a and b for each boundary of the stability categories.

Table 5.1 Description and illustrations of stability categories. (Aydan and Tokashiki 2011)

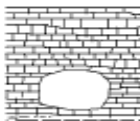



Category	Physical state	Illustration
I	Stable	
II	Local instability problems in the form of falls/sliding of individual blocks from roof and/or sidewalls. Openings are globally stable.	
III	Considerable scale of falls and sliding of rock blocks from the roof and sidewall of openings. However openings may collapse in long-term.	
IV	Opening globally unstable. In other words, it is in a total collapse state. Sinkholes appear on the ground surface.	

Table 5.2 The values of a and b in Equation 5.1 and Equation 5.2 (Aydan and Tokashiki 2011)

Category	Linear Function		Power Function	
	a	b	a	b
I-II	1,2	-60	0,001	2,4
II-III	3,0	-120	0,003	2,4
III-IV	4,3	-130	0,005	2,4

Although engineers prefer the linear formula, the power function formula is better in the sense of evaluating the observational results.

Tokashiki (2011) and Aydan and Tokashiki (2011) also proposed some stability assessment methods for the roof of shallow underground openings based on the bending theory of beams or arching theory used in structural mechanics. Particularly, the arching theory has been popular in mining engineering and many formulations are developed with the consideration of various modes of failure (Aydan, 1989; Kawamoto et. al 1991).

The observational results of the span of 38.5 m are shown in Figure 5.3 and Figure 5.4 together with proposed formulas and the data from locally collapsed caves according to linear and power functions of Aydan and Tokashiki (2011). Figure 5.5 also shows the comparative stability study with Aydan and Tokashiki, and Barton guide.

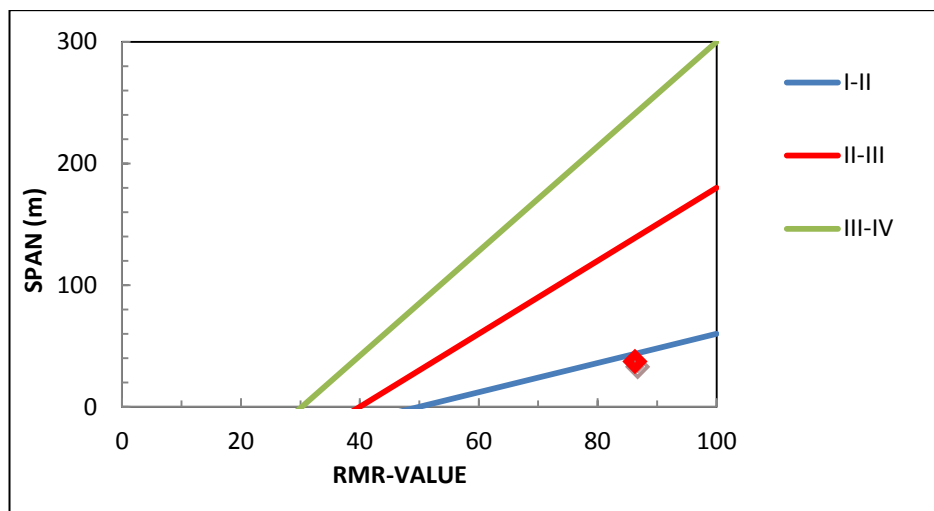


Figure 5.3 Comparison of empirical linear function for different stability categories with observations.

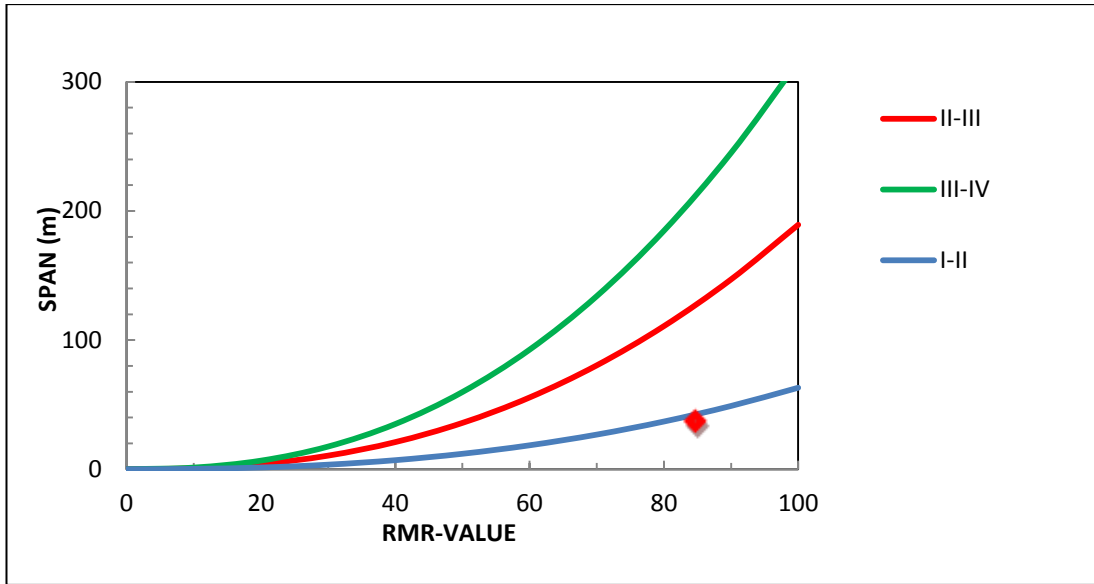


Figure 5.4 Comparison of empirical power function for different stability categories with observations.

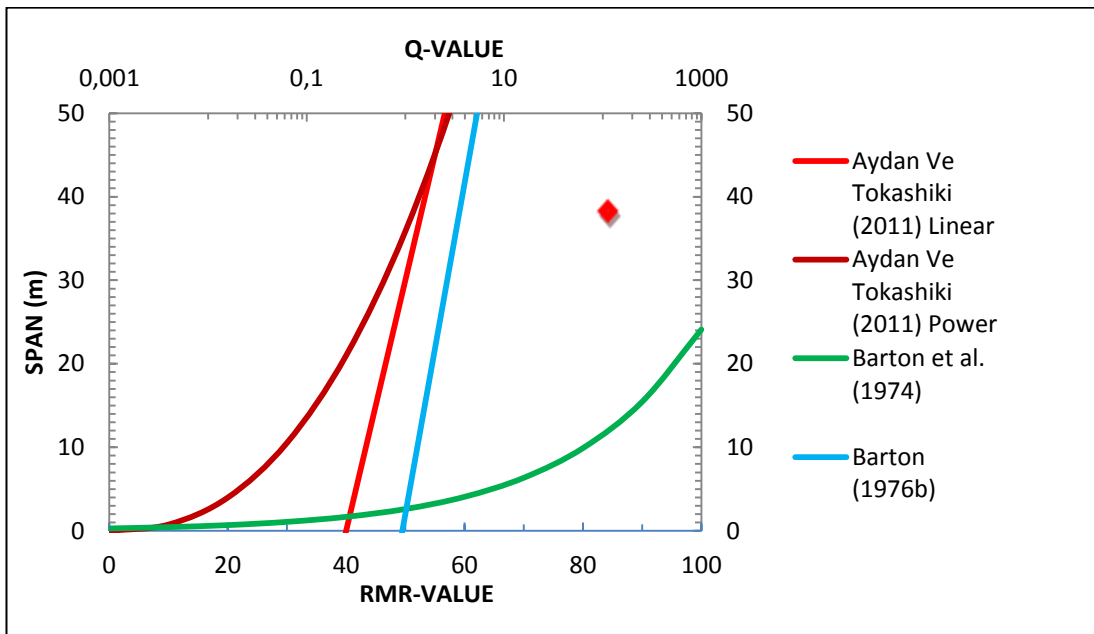


Figure 5.5 Comparison of empirical functions proposed by Aydan and Tokashiki (2011) with functions of Barton.

CHAPTER 6

ANALYTICAL APPROACHES TO ASSESS THE STABILITY

In this chapter different analytical methods are discussed to evaluate the stability of the caves.

6.1 Analysis by Euler Bernoulli Bending Theory

When a beam is subjected to transverse loads, the internal forces in any section of the beam will generally consist of a shear force (V) and a bending moment (M). The bending moment (M) creates normal stresses in the cross section, while the shear force (V) creates shearing stresses in that section.

The distribution of the normal stresses in a given section depends only upon the value of the bending moment in that section and the geometry of the section. For beam cross sections that are symmetrical about a plane perpendicular to the neutral plane, it can be shown that normal stresses experienced by the beam can be expressed as:

$$\sigma_z (y,z) = \frac{M_x (z)}{I_x} y \quad (6.1)$$

Where

σ_z is the normal stress

M_x is the bending moment about the neutral axis

y is the distance from the neutral axis to a point of interest

I_x is the moment of inertia of the cross section with respect to a centroidal axis perpendicular to the plane of the bending moment

Normal stress varies linearly with the distance from the neutral axis. This stress is compressive ($\sigma_z > 0$) above the neutral axis when the bending moment M is positive, and tensile ($\sigma_z < 0$) when M is negative for the rock beam (Figure 6.1).

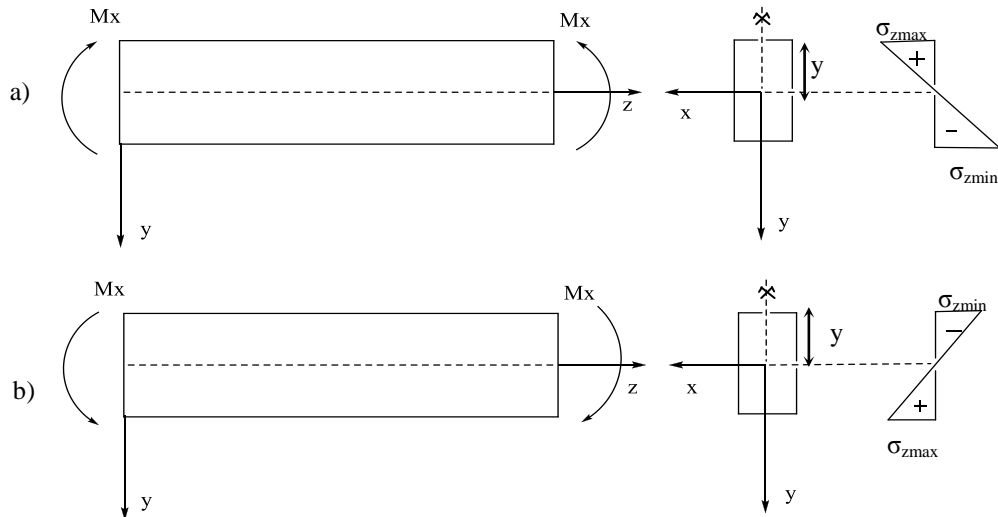


Figure 6.1 Normal stresses based on Euler Bending Theory. a) Bending moment positive, b) Bending moment negative

It should be noted here that value of the bending moment along the beam is important to calculate the normal stress. The bending moments and shear forces in Euler Bernoulli beams can often be determined directly using static balance of moments. However, for certain boundary conditions, the number of reactions can exceed the number of independent equilibrium equations. Such beams are called statically indeterminate and shear forces and bending moments can be obtained by considering the deformation of the structure involved.

Figure 6.2 shows the shear forces and bending moments at supports and midspan of the fixed end beam with a uniformly distributed load. Shear forces at supports are $\pm qL/2$ while bending moments at supports are $-qL^2/12$. Bending moment is $qL^2/24$ at midspan of the beam where shear force is zero.

If Euler Bernoulli bending theory applies to Seyrantepete caves the limit of the roof span (L) under its dead weight ($q = \gamma \times h$) can be calculated by equating the maximum tension stress to tension strength as follows:

Assumptions:

Roof rock layer is assumed as fixed end rectangular beam.

The calculations are carried out for the width of 1 m.

From Equation 6.1

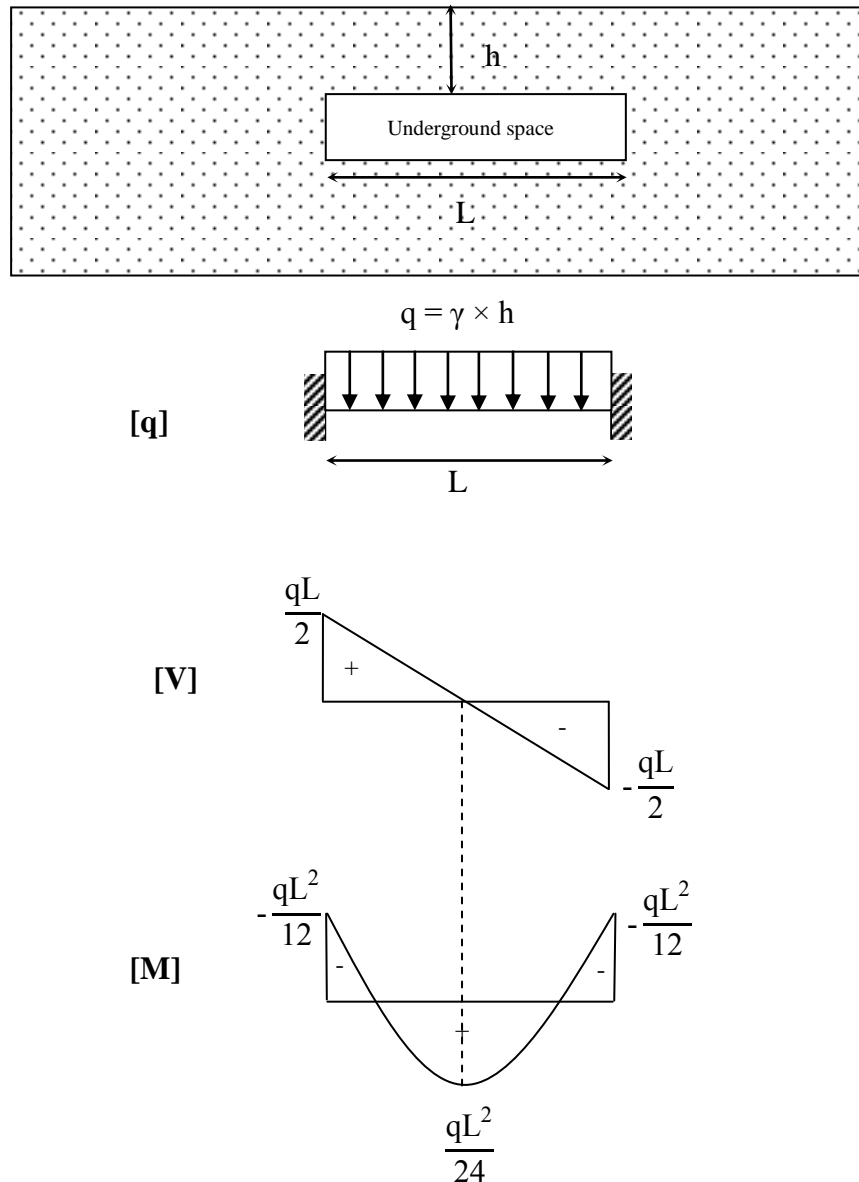


Figure 6.2 Shear forces and bending moments for a flat roof of an underground space

$$\sigma_z = \frac{M_x}{I_x} h/2 \quad (6.2)$$

where

M_x is $-qL^2/12$ that gives the maximum tension stress

q is uniformly distributed load which is equal to $\gamma \times h$

I_x is the moment of inertia of the cross section with respect to a centroidal axis perpendicular and equal to $h^3/12$

If we substitute the values of M_x and I_x into Equation 6.2

$$\sigma_{zmin} = \frac{\gamma \times L^2}{2 \times h} \quad (6.3)$$

σ_{zmin} should be equal to tension strength (σ_t). We write

$$\sigma_{zmin} = \frac{\gamma \times L^2}{2 \times h} = \sigma_t \text{ (Limit state)} \quad (6.4)$$

The limit of the roof span (L) under its dead weight is obtained from Equation 6.4 as follows:

$$L = \sqrt{\frac{2 \times h \times \sigma_t}{\gamma}} \quad (6.5)$$

Where

L is the limit of the roof span (m)

h is the roof rock layer thickness (m)

σ_t is the tensile strength of the roof layer (kPa)

γ is the unit weight of the roof rock layer (kN/m³)

Using Equation 6.5 stability assessment chart based on the relationship between RMR and roof span is obtained for $\sigma_{ti} = 380$ kPa ($\sigma_{tm} = 185$ kPa for RMR=85), $\gamma = 18,34$ kN/m³ according to bending theory (Figure 6.3). Tensile strength of the rock mass is found using the formulas suggested by Aydan et al. (2012b), Aydan and Kawamoto (2000) and Tokashiki and Aydan (2010) according to tensile strength of intact rock and the RMR value of the rock masses.

RMR value of Seyrantepe caves is between 80 and 90. As seen in Figure 6.3 limit roof span is between 12 and 15 m. for the section 1-1 of Seyrantepe caves which has roof thickness of 9 m. Limit span is lower than measured in the field. It can be said that some tension cracks and failure points will be occurred.

Stability of the roof of the widest span, which has a span of 38,5 m, is analysed using the bending theory with fixed end beam conditions. The span is 38,5 m and roof rock thickness is 9 m. for this situation. Figure 6.4 shows the shear forces and bending moments along the beam. Figure 6.5 shows the normal stresses computed in terms of bending moment. Normal stresses indicate that the compression stress (σ_c) would not

exceed the compression strength (calculated as 1982 kPa for the RMR of 85) of the rock along the beam but tension stress would exceed the tension strength of the rock around the sidewalls and at the mid-span of the opening. In other words, tensile cracking is expected above the sides and mid-span of the opening.

Tension strength of the rock mass is 185 kPa for the value of RMR of 85. Sign of the tension stresses in Figure 6.5. shows the location of tension stress according to the neutral axis of the beam. Negative tension stresses creates the tension stress at the top of the beam whereas positive tension stresses creates the tension stress at the bottom of the beam. Figure 6.5 also shows the unstable points along the beam.

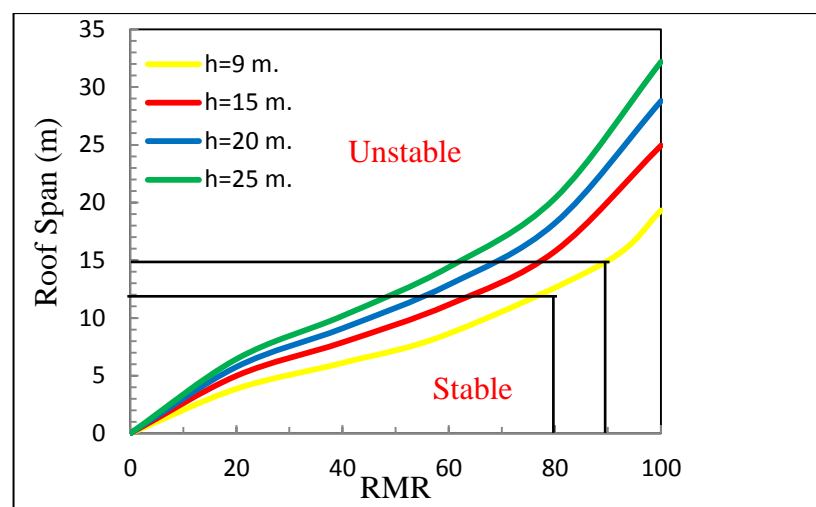


Figure 6.3 Stability assessment chart of Seyrantepe caves in terms of Euler Bernoulli Bending Theory

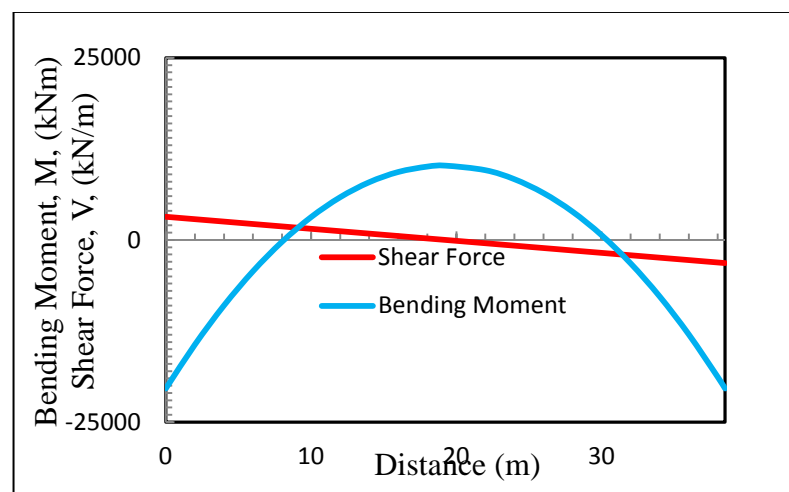


Figure 6.4 Shear forces and bending moments for the widest span of Seyrantepe caves

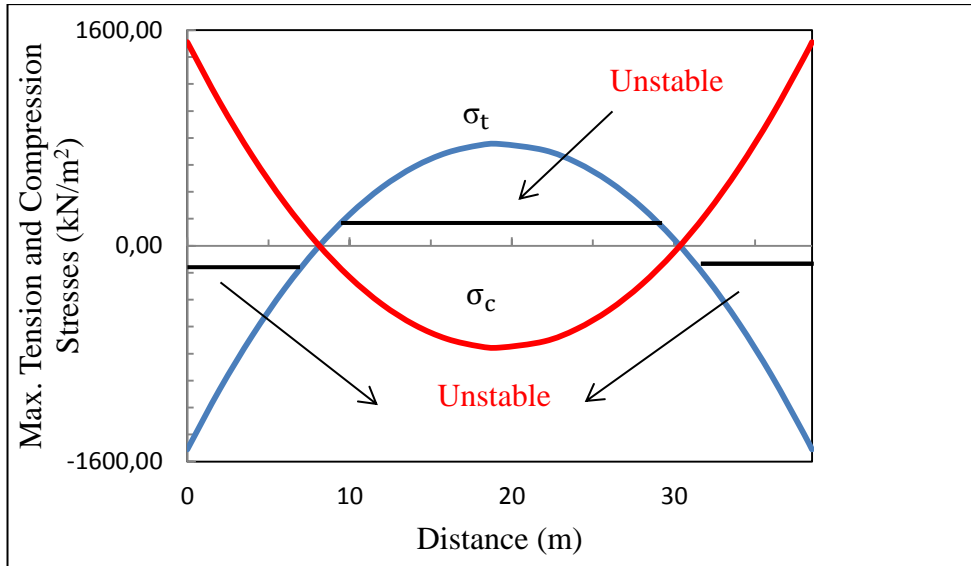


Figure 6.5 Normal stresses resulting from bending theory along the widest span of Seyrantepe caves

6.2 Analysis by Considering Shearing Stress together with Normal Stress

Shearing stress at any points of the cross section of a rectangular beam can be calculated as follows;

$$\tau_{xy} = \frac{VQ}{It} \quad (6.6)$$

Where V is shear force applied to beam cross section, I is the moment of inertia of the cross section, t is equal to the width b of the beam and where Q is the first moment with respect to the neutral axis of the shaded area A (Figure 6.6).

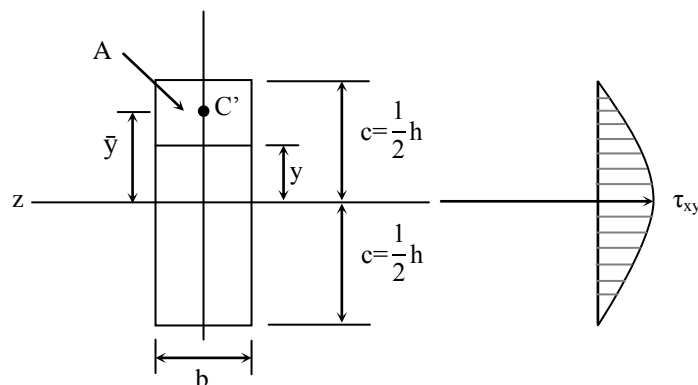


Figure 6.6 Shearing stress distribution of the rectangular beam

Observing that the distance from the neutral axis to the centroid C' of A is $\bar{y} = \frac{1}{2}(c+y)$, and Q is written as follows;

$$Q = A\bar{y} = b(c-y) \frac{1}{2}(c+y) = \frac{1}{2}b(c^2 - y^2) \quad (6.7)$$

If $I = bh^3/12 = \frac{2}{3}bc^3$, $Q = \frac{1}{2}b(c^2 - y^2)$, and $A = 2bc$ substitute into equation 6.6 shearing stresses can be calculated at any points of the cross section of a rectangular beam as follows;

$$\tau_{xy} = \frac{3V}{2A} \left(1 - \frac{y^2}{c^2} \right) \quad (6.8)$$

Equation 6.8 shows that the distribution of shearing stresses in a transverse section of a rectangular beam is parabolic (Figure 6.6). Shearing stresses are zero at the top and bottom of the cross section (when y is equal to $\pm c$). Making $y = 0$ in Equation 6.8 the maximum shearing stress in a given section of rectangular beam is calculated as ;

$$\tau_{\max} = \frac{3V}{2A} \quad (6.9)$$

Shearing stresses together with normal stresses cause the state of biaxial stress at applied point. Stresses must provide some safety conditions when designing and checking the section. Some criterion regarding the actual mechanism of failure of the material must first be established, which will make it possible to compare the effects of both states of stress on the material. For this situation, principal stresses play an important role to determine points of failure of the section.

Principal stresses under given normal stresses and shearing stresses in a beam can be calculated as follows;

$$\sigma_1 = \frac{1}{2} \left[\sigma + \sqrt{\sigma^2 + 4\tau^2} \right]$$

$$\sigma_3 = \frac{1}{2} \left[\sigma - \sqrt{\sigma^2 + 4\tau^2} \right]$$

To predict whether the rock mass will yield at some critical point under given loading condition, principal stresses should be determined at that point and checked with a known failure criterion. In this part maximum and minimum principal stresses were calculated for the span of 38.5 m being the widest span of the cave. Table 6.1 shows the principal stresses in the side of the fixed end beam. Normal stresses were obtained from equation 6.2 and shearing stresses from equation 6.8. Mohr Coulomb failure criterion was used to determine the points of failure.

According to the Mohr Coulomb failure criterion for the state of plain stress

$$\frac{\sigma_1}{\sigma_t} + \frac{\sigma_3}{\sigma_c} = \beta$$

Where:

σ_1 is maximum principal stress

σ_3 is minimum principal stress

σ_t is axial tension strength

σ_c is uniaxial compression strength

If

$\beta < 1$ stress state is safe

$\beta = 1$ stress state is limit

$\beta > 1$ stress state is unsafe

Here, tension strength of rock mass is taken as 185 kPa, unconfined compression strength is taken as 1982 kPa. Table 6.1 also presents the stress state of the section. Directions of the maximum and minimum principal stresses in the cross section near the fixed support are shown in Figure 6.7.

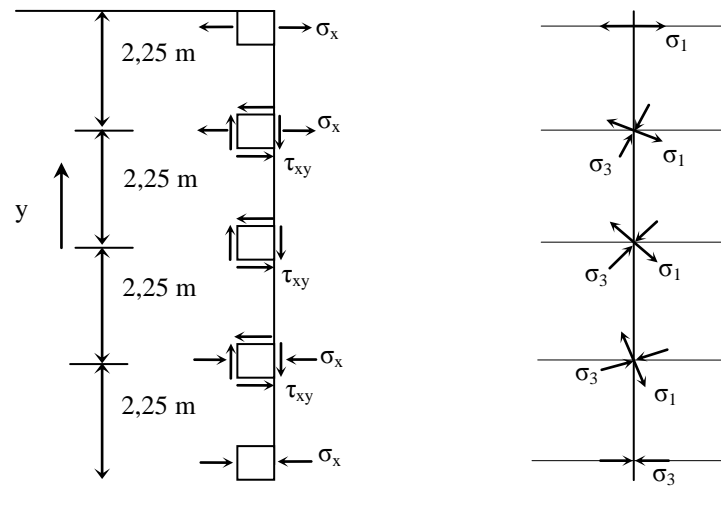


Figure 6.7 Principal stress of the rectangular beam

Table 6.1 Calculation table to determine the stress state in the cross section near the fixed support

y	c	Moment (kNm)	Normal Stress (kPa)	Shearing Stress (kPa)	Max Principal Stress, σ_1 , (kPa)	Min Principal Stress, σ_3 , (kPa)	β	Stress State
4,50	4,5	-20388,35	-1510,25	0,00	0,00	-1510,25	8,164	Unsafe
2,25	4,5	-20388,35	-755,12	397,18	0,53	-755,65	4,085	Unsafe
0,00	4,5	-20388,35	0,00	529,57	23,01	-23,01	0,136	Safe
-2,25	4,5	-20388,35	755,12	397,18	755,65	-0,53	0,384	Safe
-4,5	4,5	-20388,35	1510,25	0,00	1510,25	0,00	0,762	Safe

6.3 Pillar Analysis

Pillars are key structural columns that are commonly applied in underground space. They are usually made of in situ intact rock and do not have additional reinforcements. Their main function is to provide temporary or permanent support for the weight of overburden material between adjacent underground openings and ore ceiling of drilling rooms during excavation and mining (Deng et.al, 2003). Due to their significance in safe, their design have been investigated by a number of researchers and engineers over the past few decades.

In 1980, field studies conducted by the US Bureau of Mines had developed the classic pillar design methodology. It consisted of three steps (Mark, 2006):

1. Prediction of the pillar strength
2. Prediction of the pillar load
3. Calculating the pillar safety factor.

The average pillar load can be estimated by tributary-area theory. Base on this theory, each individual pillar is assumed to carry the weight of the overburden immediately above it. In the other words, a pillar uniformly supports the weight of rock overlying the pillar and one-half the width of rooms or entries on each side of the pillar (Peng, 1978). Figure 6.8a shows a cross section of parallel underground spaces being excavated using long rooms and rib pillars. Room spans and pillar spans are w_o and w_p respectively. For a sufficiently extensive set of rooms and pillars, a representative segment of the structure is as shown in Figure 6.8b. Considering the requirement for equilibrium of any component of the structure under the internal forces and unit thickness in the antiplane direction, the free body shown in Figure 6.8c.

Figure 6.8c yields the following equation

$$\sigma_p w_p = p_{zz} (w_o + w_p)$$

or

$$\sigma_p = p_{zz} (w_o + w_p) / w_p$$

In this expression, σ_p is the average axial pillar stress, and p_{zz} is the vertical normal component of the pre-excavation stress field. The width ($w_o + w_p$) of the representative free body of the pillar structure is often described as the area which is tributary to the representative pillar. The term of tributary area method is therefore used to describe this procedure for estimating the average state of axial stress in the pillar (Brady and Brown, 2004).

Pillar geometry affects the stress concentration. In the same cross section, for two pillars, angular one takes more stress concentration than rounded one. Figure 6.9 summarizes the average pillar stress for the different pillar geometry (Karpuz and Hindistan, 2008).

Pillar strength can be defined as the maximum resistance of a pillar to axial compression. Empirical evidence suggests that pillar strength is related to both its volume and its shape (Brady and Brown, 2004). Numerous formulas have been developed that can be used to estimate the strength of pillars, which Table 6.2 shows the most applicable of them. Each of these formulas estimates the pillar strength in terms of two variables; width to height ratio and in situ strength.

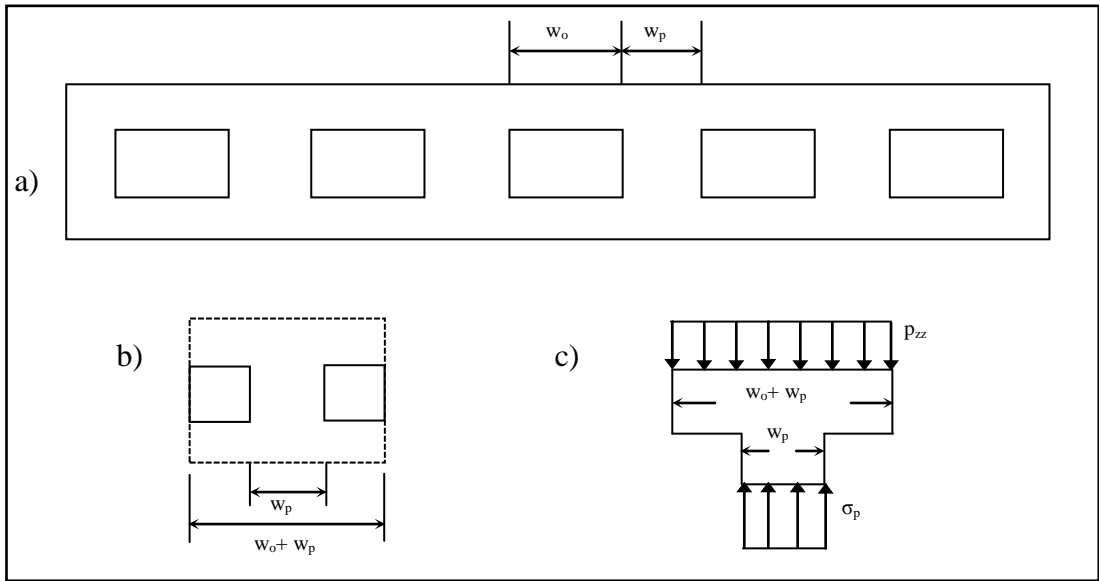


Figure 6.8 Bases of the tributary area method for estimating average axial pillar stress (Brady and Brown, 2004)

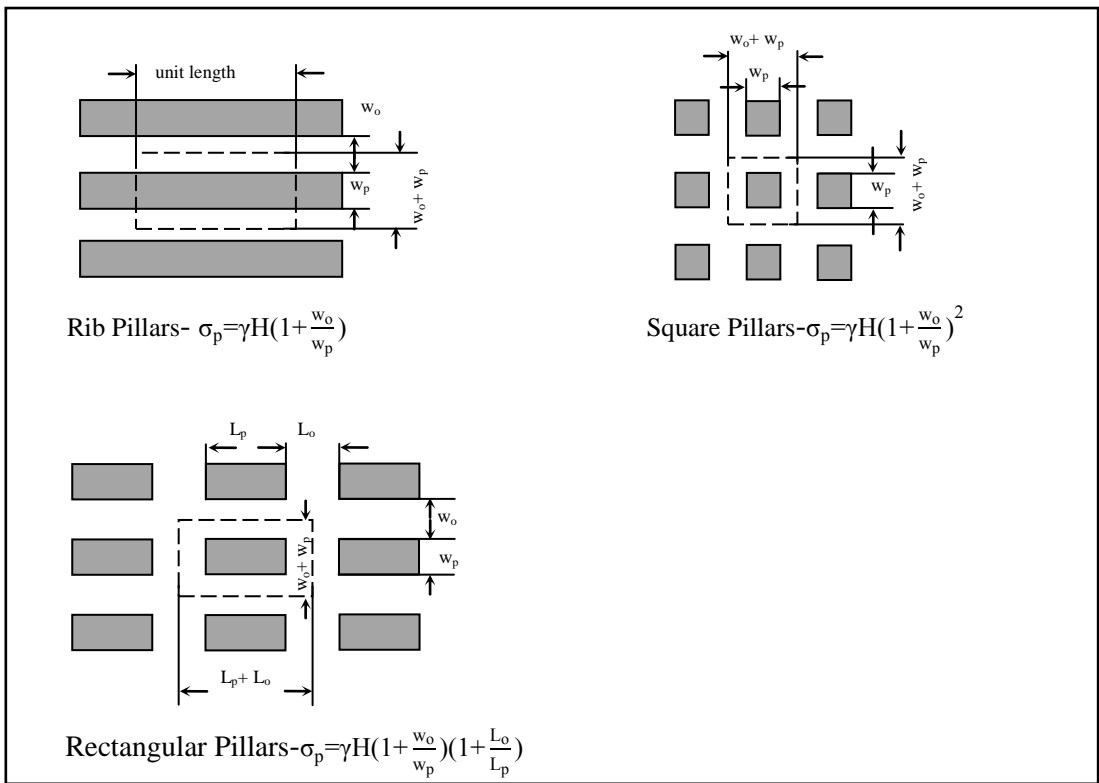


Figure 6.9 Average pillar strength for different shaped pillars (Karpuz and Hindistan, 2008).

Table 6.2 Most applicable of empirical strength formula for pillars (Karpuz and Hindistan, 2008)

Reference	Equation	Factor of Safety
Salomon and Munro (1967)	$c_p = c_1 \left(\frac{W^{0,46}}{H^{0,66}} \right)$	1,6
Hustrulid and Swanson (1981)	$c_p = \frac{K}{H^{0,5}} (W/H)^{0,5}$	-
Obert and Duvall (1946,1967)	$c_p = c_1 (0,778 + 0,222 \frac{W}{H})$	1,5 - 2,0
Holland and Gaddy (1964)	$c_p = \frac{K}{H} W^{0,5}$	1,8 - 2,0
Bieniawski (1968,1981)	$c_p = c_1 (0,64 + 0,36 \frac{W}{H}^\alpha)$	2,0
Greenwald et.al. (1939)	$c_p = c_1 \left(\frac{W^{0,83}}{H^{0,66}} \right)$	-

Where

c_1 is the sample in situ strength of critical size

c_p is the pillar strength

W is pillar width

K is the strength of a unit cube of sample

H is pillar height

Pillar design is typically performed by predicting the strength and the stress of the pillars, and then sizing the pillars so that an adequate margin exists between the expected pillar strength and stress. Because the uniaxial compressive strength of the rock plays an important role in pillar instability, the stability of a pillar can be evaluated by calculating a factor of safety (FS), which is the ratio of the average strength (c_p) to the average stress (σ_p) in the pillar ($FS = c_p / \sigma_p$). Theoretically, the FS value greater than 1 means that the pillar is stable, while the FS value lower than 1 means unstable. Sometimes, these methods, however, are questionable because failures in pillars did occur even though the failed pillars had been considered stable. Thus researchers focus on this subject defined their own FS value in their related equations. So every equation in Table 6.2 should be used by considering their own factor of safety value to determine the pillar stability.

Here pillar between cave no 4 and 5 which is found critical in FEM analysis was discussed for a 1m. unit length. The width and height of the pillar are 1,94 m and 5,6 m, respectively. Room span (w_o) was obtained as 26,3 m. by taking average value

of adjacent spans. In situ strength of rock mass had been found as 1,982 MPa for RMR=85 from the relations suggested by Aydan and Tokashiki (2012).

The tributary area analysis of this pillar is as follows:

Pre-excavation stress:

$$p_{zz} = \gamma H = 18,34 \times 9 = 0,165 \text{ MPa}$$

Average axial pillar stress for long rib pillars:

$$\sigma_p = p_{zz} (1 + w_0) / w_p$$

$$\sigma_p = 0,165 (1 + 26,3) / 1,94 = 2,322 \text{ MPa}$$

If pillar strength (c_p) is calculated by the empirical expression suggested by Salomon and Munro (1967) in Table 6.2, it will be found as follows

$$c_p = c_1 \left(\frac{W^{0,46}}{H^{0,66}} \right) = 1,982 \left(\frac{1,94^{0,46}}{9^{0,66}} \right) = 0,631 \text{ MPa}$$

Factor of safety is found as

$$FS = \frac{c_p}{\sigma_p} = \frac{0,631}{2,322} = 0,27 < 1,6$$

CHAPTER 7

CONCLUSION AND RECOMMENDATIONS

In this thesis, stability assessment of Gaziantep Seyrantepe caves was carried out and its implications in geotechnical engineering were discussed. To determine the geotechnical parameters of the rock mass as input parameters for the calculations, experimental and theoretical studies suggested by various researchers were used. Integrated numerical, empirical and analytical methods were undertaken to investigate the short term stability of the caves.

The experimental results and visual site characterization study showed that, although limestone surrounding the caves is a very good quality rock mass, it is a very weak rock in terms of intact rock strength. The strength of the rock was drastically reduced under saturated conditions. It is expected that the alteration and the process of freezing-thawing accelerates further degradation of the rock and more detailed studies are recommended for long term stability in view of the effects of degradation due to wetting-drying and freezing-thawing processes and the time-dependent characteristics of the surrounding rock mass.

Back analysis results gave lower strength parameters compared with Mohr Coulomb criteria. While the lowest strength parameters were obtained from Hoek Brown criteria, Mohr-Coulomb criteria gave the highest strength parameters. It can be said that Hoek Brown is on the safe side for this massive rock

Numerical analysis showed that adjacent spans effected the stability and failure process. When considered the single isolated opening, the factor of safety against failure was calculated greater than that of for adjacent caves. Tension cut off points occurred at the midspan of the caves for single isolated opening. When considered the adjacent caves, tension cut off points developed towards the weak pillar.

Empirical methods to assess the stability and the rock support estimation indicated that RMR classification system did not suggest any support except for occasional

spot bolting and RMR value gave the idea for stand up time. Q system recommended the spot bolting and systematic bolting.

As mentioned before empirical approaches commonly help to determine the rock support and generally use for this purpose. They are very useful for first estimation of rock supports but for rock masses with swelling and squeezing ground, none of the rock mass classification system works well. They do not exactly consider the stress parameters, which is vital. For more accurate and optimum solution to estimate the rock support system, numerical analysis technique is suggested. For the analysis through numerical approach, initial values of rock supports for the simulation are needed. In this regard, suggested values of rock supports from the empirical approaches like RMR, Q system, RMI system, would be better choice and are used. Various combination of lining (shotcret, concrete, RCC) and bolts are analyzed through numerical analysis and have eventually estimated the optimum values of support combinations which provides the required degree of safety and have relatively least cost. In numerical analysis, this requirement is achieved by reducing the maximum number of yielded elements.

Cave no 5 placed over section 1-1 whose roof span is 38,5 m. remained stable or partial stable according to the empirical functions proposed by Aydan and Tokashiki (2011). It is thought that this situation corresponds to the stability categories observed when caves were excavated. Hence, it can be said that empirical functions proposed by Aydan and Tokashiki (2011) are suitable for this cave.

Empirical function proposed by Barton et. al (1974) gave more conservative results compared with approach of Aydan and Tokashiki (2011). According to Barton et. al (1974) spans which are more than 15 m. remained unstable for RMR of 85. This approach is more reliable for preliminary design of underground openings. Because, spans are smaller than approach of Aydan and Tokashiki (2011).

According to the bending theory limit roof span is between 12 and 15 m for the section 1-1 of Seyrantepe caves which has roof thickness of 9 m. The rock mass behaves elastically up to these values. If the span is greater, the rock mass will yield and plastic points will take place. Bending theory indicates that the tensile stress would exceed the tensile strength of the rock both at the top of the rock beam near

sidewall and at the mid span of the opening near the roof. Plastic tensile points are expected for these locations. This conclusion is in accordance with FEM analysis.

By considering both the normal stress and shearing stress yielded points along the height of the cross section were obtained. The results are quite compatible with FEM analysis

Analytical analysis of pillar between cave no 4 and 5 gave lower factor of safety than that of suggested by Salomon and Munro (1967). In other words pillar stress is greater than pillar strength. This clearly implies that some cracking will be occur, and the result is in accordance with FEM analysis.

REFERENCES

- Akgün, H., and Koçkar, M.K. (2004). Design of anchorage and assessment of the stability of openings in silty, sandy limestone: a case study in Turkey. *International Journal of Rock Mechanics & Mining Sciences*, **41**, 37-49.
- Aydan, Ö. (1989). The stabilisation of rock engineering structures by rockbolts. PhD Thesis, Nagoya University.
- Aydan Ö., and Kawamoto T. (2000). Assessing mechanical properties of rock masses by RMR rock classification method. *GeoEng. 2000 Symposium*, Sydney.
- Aydan Ö., and Tokashiki N. (2011). A comparative study on the applicability of analytical stability assessment methods with numerical methods for shallow naturel underground openings. *IACMAG*, Melbourne, Australia.
- Aydan Ö., Geniş M., and Tokashiki N. (2012). Some consideration on yield (failure) criteria in rock mechanics. *46th US Rock Mechanics/Geomechanics Symposium*.Chicago.
- Barton, N.R., Lien, R., and Lunde, J. (1974). Engineering classification of rock masses for the design of tunnel support. *Rock Mechanics*, **6(4)**, 189-239.
- Barton N. (1976a). The shear strenght of rock and rock joints. *International Journal of Rock Mechanics & Mining Sciences*, **13(10)**, 189-239.
- Barton N. (1976b). Unsupported underground opening. *Rock Mechanics Discussion Meeting, Swedish Rock Mechanics Research Foundation*. Stockholm.
- Baykasoğlu, A., Güllü, H., Çanakçı, H., and Özbakır, L. (2008). Prediction of compressive and tensile strength of limestone via genetic programming. *Expert Systems with Applications*, **35**, 111-123.

- Bieniawski, Z.T. (1989). *Engineering rock mass classifications*. New York: Wiley.
- Brady B.H.G., and Brown E.T. (2004). *Rock mechanics for underground mining*. London: Chapman & Hall.
- Canakci, H. (2007). Collapse of caves at shallow depth in gaziantep city center, Turkey: a case study. *Environmental Geology*, **53**, 915-922.
- Canakci, H., and Gullu, H. (2008). Development of a hazard assessment model for near surface caves in limestone. *Engineering Geology*, **105**, 102-107.
- Coduto D. P., Yeung M.C.R., and Kitch W.A. (2010). *Geotechnical engineering: principles and practices*. 2nd. edition. Prentice Hall.
- Coskun, B., and Coskun, B. (2000). The Dead Sea Fault and related subsurface structures, Gaziantep Basin, southeast Turkey. *Geological Magazine*, **137 (2)**, 175-192.
- Deng, J., Yue, Z.Q., Tham, L.G., and Zhu, H.H. (2003). Pillar design by combining finite element methods, neural networks and reliability: a case study of the Fenghuangshan Copper Mine, China. *International Journal of Rock Mechanics and Mining Sciences*, **40(4)**, 585–599.
- Hatzor, Y.H., Wainshtein, I., and Mazor, D.B. (2010). Stability of shallow karstic caverns in block rock masses. *International Journal of Rock Mechanics & Mining Sciences*, **47**, 1289-1303.
- Hoek E., and Brown E.T. (1980a). *Underground Excavations in Rock*. London: Institution of Mining and Metallurgy.
- Hoek, E., and Brown, E.T. (1980b). Empirical strength criterion for rock masses. *Journal of Geotechnical Engineering (ASCE)*, **106**, 1013-1035.
- Hoek, E. (1994). Strength of rock and rock masses. *ISRM News J*, **2(2)**, 4-16.
- Hoek, E., Kaiser, P.K., and Bawden. W.F. (1995). *Support of underground excavations in hard rock*. Rotterdam: Balkema.

Hoek, E., and Brown, E.T. (1997). Practical estimates of rock mass strength. *International Journal of Rock Mechanics & Mining Sciences*, **34(8)**, 1165-1186.

Hoek E., Carranza-Torres C.T., and Corkum B. (2002) Hoek-Brown failure criterion-2002 edition. *International Proceedings of the 5th North American Rock Mechanics Symposium. Toronto, Canada*, **1**, 267–273.

Hoek, E., and Diederichs, M. (2006). Empirical estimates of rock mass modulus. *International Journal of Rock Mechanics & Mining Sciences*, **43**, 203–215.

Hoek, E. Practical rock engineering. Rocscience:Canada.

Karpuz C., ve Hindistan M.A. (2008). Kaya mekaniği ilkeleri, uygulamaları. 2. Basım. Ankara: TMMOB Maden Mühendisleri Odası Yayınları.

Köksal, E., Köksal, H.O., and Yıldırım, H. (2004). Eksenel basınç altında beton biriket yığıma prizmaların sonlu eleman analizi. *İMO Teknik Dergi*, **218**, 3249-3265.

Marinos, P., and Hoek, E. (2000). GSI – A geologically friendly tool for rock mass strength estimation. *Proc. GeoEng2000 Conf., Melbourne*.

Mark, C. (2006). The evolution of intelligent coal pillar design: 1981–2006. *International Proceedings of the 25th International Conference on Ground Control in Mining*, Morgantown, West Virginia University, USA.

Nilsen, B., and Palmstrøm, A. (2000). *Engineering Geology and Rock Engineering, Handbook No 2*. Oslo: Norwegian Group for Rock Mechanics.

Peng, S.S. (1978). *Coal Mine Ground Control*. New York: John Wiley & Sons.

Terlemez I., Şentürk K., Sümengen M., and Oral A. (1997). Türkiye jeoloji haritaları. No: 45 Jeoloji Etütleri Dairesi, Ankara.

Tolun N. (1975). Türkiye Jeoloji Haritası, Hatay. Ankara: MTA Enstitüsü Yayınları.